iScience

CellPress
OPEN ACCESS

Article

Activated platelets facilitate hematogenous metastasis of breast cancer by modulating the PDGFR-β/COX-2 axis

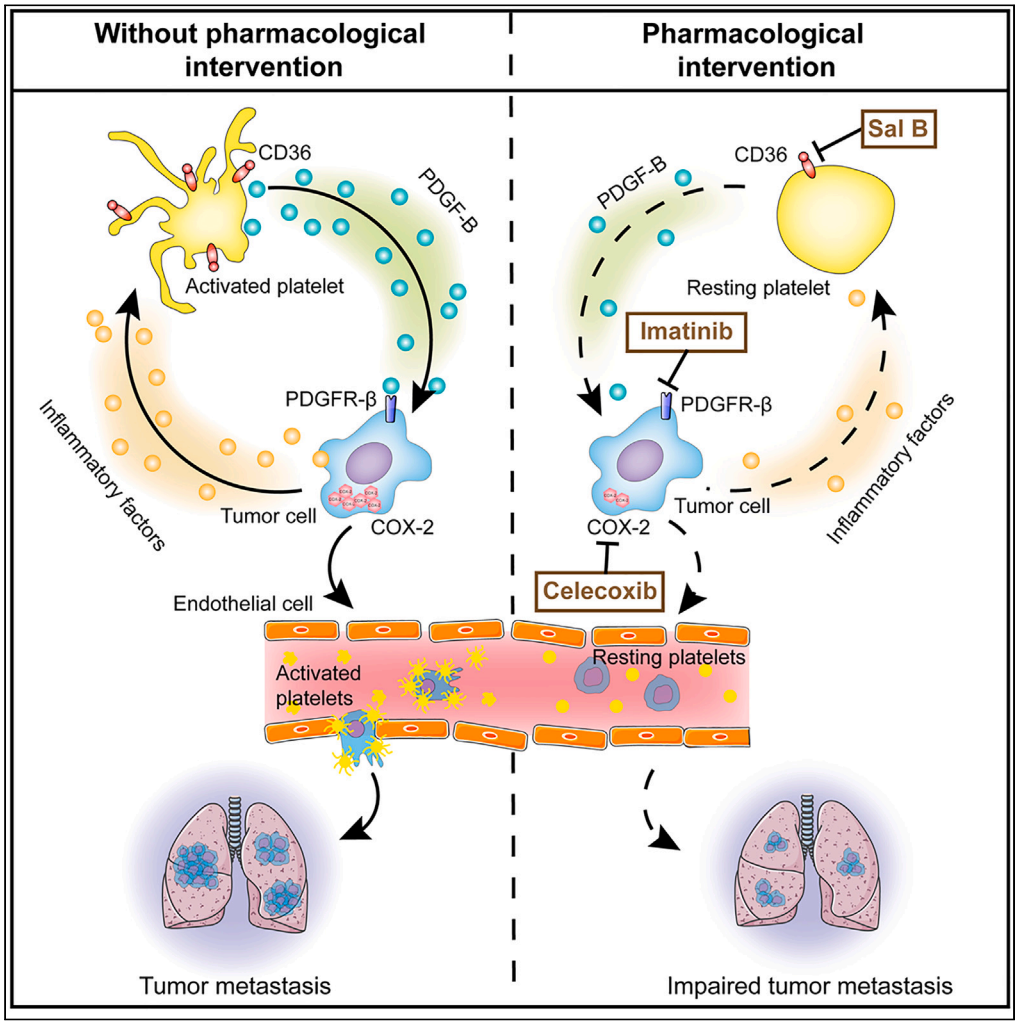

Yu Tang, Cheng Qian, Yueke Zhou, ..., Aiyun Wang, Yang Zhao, Yin Lu

wangaiyun@njucm.edu.cn (A.W.)
y.zhao@njucm.edu.cn (Y.Z.)
luyingreen@njucm.edu.cn (Y.L.)

Highlights

Platelets promote cancer metastasis through modulating PDGFR-β/COX-2 signaling cascade

Cancer cells result in the activation of platelets through augmenting CD36 expression

Co-inhibition of COX-2 and CD36 restricts the metastasis of breast cancer

Tang et al., iScience *26*, 107704
September 15, 2023
https://doi.org/10.1016/j.isci.2023.107704

iScience

CellPress
OPEN ACCESS

Article

Activated platelets facilitate hematogenous metastasis of breast cancer by modulating the PDGFR-β/COX-2 axis

Yu Tang,[1,6] Cheng Qian,[1,6] Yueke Zhou,[1] Chang Yu,[2] Mengyao Song,[1] Teng Zhang,[1] Xuewen Min,[3] Aiyun Wang,[1,4,5,7,*] Yang Zhao,[1,2,*] and Yin Lu[1,4,5,*]

SUMMARY

Platelets have been widely recognized as a bona fide mediator of malignant diseases, and they play significant roles in influencing various aspects of tumor progression. Paracrine interactions between platelets and tumor cells have been implicated in promoting the dissemination of malignant cells to distant sites. However, the underlying mechanisms of the platelet-tumor cell interactions for promoting hematogenous metastasis are not yet fully understood. We found that activated platelets with high expression of CD36 were prone to release a plethora of growth factors and cytokines, including high levels of PDGF-B, compared to resting platelets. PDGF-B activated the PDGFR-β/COX-2 signaling cascade, which elevated an array of pro-inflammatory factors levels, thereby aggravating tumor metastasis. The collective administration of CD36 inhibitor and COX-2 inhibitor resolved the interactions between platelets and tumor cells. Collectively, our findings demonstrated that targeting the crosstalk between platelets and tumor cells offers potential therapeutic strategies for inhibiting tumor metastasis.

INTRODUCTION

The high lethality of tumors has been accepted to be closely associated with metastasis.[1] Platelets, classified as small non-nuclear hematopoietic cells, play a crucial role in hemostasis and thrombosis. They are considered the first host cells encountered by tumor cells during the hematogenous metastasis process.[2,3] In the development of malignant tumors, multiple types of signaling crosstalk and dynamic cascade interactions exist between platelets and tumor cells. On one hand, platelets can resist the damage of blood flow shear force by adhering to the tumor cell surface. In this regard, platelets play pivotal roles in propelling tumor cell extravasation, intensifying the interactions between tumor cells and endothelial cells (ECs), and thus accelerating tumor metastasis.[4,5] On the other hand, tumor cells have been revealed to have profound consequences on the number and activation state of platelets, as well as platelet aggregation.

The tumor cell-mediated platelet activation process can be categorized into two modes, namely direct activation and indirect activation, when tumor cells enter the circulation.[6,7] In the direct mode, platelet activation occurs through direct contact between the surface mediators of the platelet membrane and circulating tumor cells (CTCs). Representative molecules involved in this mode include P-selectin, integrins, and glycoproteins.[8,9] The indirect mode refers to the activation of platelets triggered by metabolites secreted from tumor cells. Critical metabolites involved in this mode include thrombin, adenosine diphosphate (ADP), thromboxane A2 (TXA2), etc. In the network of tumor cell-platelet interactions, platelets, and tumor cells tend to contact and interact with each other and collaboratively metastasize to the distal organs in the circulating blood.[10–12]

Cyclooxygenase (COX), also known as prostaglandin-endoperoxide synthase, is a crucial bifunctional enzyme due to its dual COX and catalase activities. It also serves as a fundamental enzyme responsible for catalyzing the conversion of arachidonic acid into prostaglandins.[13] COX consists of two distinct isoenzymes, including COX-1 and COX-2.[14] Notably, the expression level of COX-2 as an inducible enzyme in normal cells is extremely low. However, upon inflammation, cellular stimulation can cause a remarkable elevation in the expression level of COX-2, ranging from 10 to 80 times higher than the normal level. This elevated expression level subsequently leads to increased expression levels of PGE2, PGI2, and PGE1 at the site of inflammation, resulting in a striking inflammatory response and tissue damage.[15–17] In the tumor

[1]Jiangsu Key Laboratory for Pharmacology and Safety Evaluation of Chinese Materia Medica, School of Pharmacy, Nanjing University of Chinese Medicine, Nanjing 210023, China
[2]Department of Biochemistry and Molecular Biology, School of Medicine & Holistic Integrative Medicine, Nanjing University of Chinese Medicine, Nanjing 210023, China
[3]Department of Outpatient, Jurong People's Hospital, Zhenjiang 212400, China
[4]Jiangsu Joint International Research Laboratory of Chinese Medicine and Regenerative Medicine, Nanjing University of Chinese Medicine, Nanjing 210023, China
[5]Jiangsu Collaborative Innovation Center of Traditional Chinese Medicine (TCM) Prevention and Treatment of Tumor, Nanjing University of Chinese Medicine, Nanjing 210023, China
[6]These authors contributed equally
[7]Lead contact
*Correspondence: wangaiyun@njucm.edu.cn (A.W.), y.zhao@njucm.edu.cn (Y.Z.), luyingreen@njucm.edu.cn (Y.L.)
https://doi.org/10.1016/j.isci.2023.107704

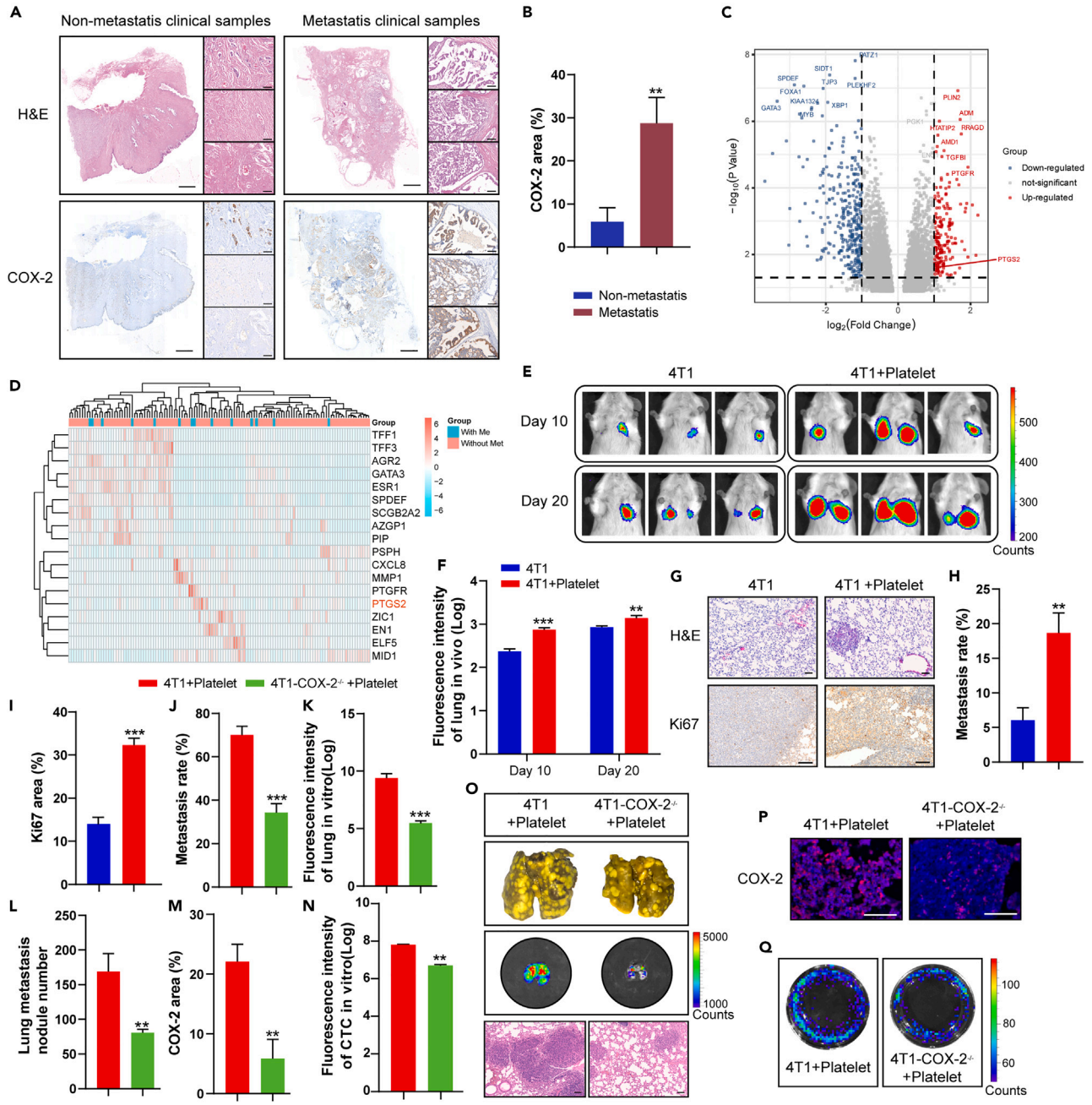

Figure 1. Platelet promotes hematogenous metastasis of breast cancer in a COX-2-dependent manner

(A) Representative images for H&E and IHC staining of COX-2 in the tumor samples from breast cancer patients.

(B) Quantification of relative COX-2 positive area (n = 9–11).

(C) Volcano plots of differentially expressed genes in the breast cancer patients with or without metastasis in GSE2603.

(D) Heatmap of differentially expressed genes in the breast cancer patients with or without metastasis in GSE2603.

(E) Representative bioluminescent images of metastasis in the mice intravenously receiving 4T1 breast cancer cells on days 10 and 20.

(F) Quantification of the bioluminescence imaging signals for the lung metastasis (n = 5).

(G) Representative images of H&E and IHC staining of Ki67 in the lung tissues.

(H) Metastatic rates of 4T1 tumor-bearing mice (n = 5).

(I) Quantification of the percentage of $Ki67^{+}$ cells in the visual field (n = 5).

(J) Metastatic rates of 4T1-platelet and 4T1-$COX\text{-}2^{-/-}$-platelet mice (n = 5).

(K) Quantification of the bioluminescence imaging signals of the harvested lungs (n = 5).

(L) Quantitative analysis of the number of lung metastatic nodules in the 4T1-platelet mice (n = 5).

Figure 1. *Continued*

(M) Quantification of COX-2 positive fields in the lung metastatic nodules (n = 5).

(N) Bioluminescence quantification of luciferase-positive CTC colonies (n = 5).

(O) Representative images of the metastatic nodules on the lung surface, bioluminescent images of metastasis in the harvested lungs and H&E staining of lung tissues in the 4T1-platelet mice.

(P) Representative images of lung tissue sections in the 4T1-platelet mice stained for COX-2 (red).

(Q) Representative bioluminescent images of luciferase-positive CTC colonies isolated from whole blood in the 4T1-platelet mice.

Data are presented as Mean ± SD. *p < 0.05, **p < 0.01, ***p < 0.001.

inflammatory microenvironment (TIM), a high expression profile of COX-2 has been observed within tumors. This upregulation of COX-2 facilitates and promotes tumor metastasis.[18] More interestingly, the presence of platelets exerts profound effects on orchestrating the formation of TIM.[19] However, whether COX-2-driven tumor metastasis is mediated through activated platelets and the underlying mechanisms remain elusive.

It has been established that platelets are the smallest circulating cells, with a diameter ranging from 2 to 5 μm. They exhibit a biconvex, discoid shape and, when inactive, feature open canalicular systems—an intricate plethora of membranes that interact with the extracellular space, dense granules, α-granules, mitochondria, and lysosomes.[20,21] CD36, also called the scavenger receptor B2, is recognized as a multifunctional receptor exhibiting widespread expression in various organs. It has been elucidated that CD36 is critically involved in the uptake of long-chain fatty acids, the predominant metabolic substrate in myocardial tissue.[22] It has been verified that CD36 is highly expressed in activated platelets.[23] More interestingly, the highly expressed CD36 is strongly linked to the morphology and function of activated platelets.

The present study established a co-culture system of platelets and tumor cells to investigate their interactions. It was illustrated that conditioned media (CM) from tumor cells boosted the activation of platelets by exerting an impact on CD36 receptors in the platelets. This activation subsequently led to the secretion of high levels of platelet-derived growth factor (PDGF)-B. PDGF-B contributed to activating the PDGFR-β/COX-2 signaling pathway in the tumor cells, further aggravating the progression of tumor hematogenous metastasis. Inhibition of CD36 by Salvianolic acid B (Sal B) reversed the platelet hyperactivity in the mice intravenously receiving platelets and tumor cells. It was also found that the impact of celecoxib on tumor metastasis, a classic COX-2 inhibitor, was significantly enhanced in the presence of Sal B. This finding supported the fact that celecoxib, in combination with the CD36 inhibitor in the mice, intravenously receiving platelets and tumor cells with the high expression level of COX-2, synergistically prevented tumor hematogenous metastasis.

RESULTS

Platelet promotes hematogenous metastasis of breast cancer in a COX-2-dependent manner

To investigate the role of COX-2 in influencing metastasis of breast cancer, we firstly examined the protein expression of COX-2 in 20 breast cancer patient samples, among which 11 patients were found with metastasis. Interestingly, the IHC staining results showed that the protein expression of COX-2 in the metastatic breast cancer samples was significantly higher than that in the non-metastatic breast cancer samples (Figures 1A and 1B). In this regard, we further performed bioinformatics analysis to explore the potential association between breast cancer metastasis and COX-2 expression level. As previously described,[24] Gene Expression Omnibus (GEO, http://www.ncbi.nlm.nih.gov/geo/) database was applied to analyze the transcriptome array of the representative clinical samples. The differential gene expression in GSE2603 transcriptome chips was visualized by volcano plots (Figure 1C). Likewise, the heatmap analysis showed the differentially expressed genes between the non-metastatic group and the metastatic group (Figure 1D). Of note, it was demonstrated that the extent of breast cancer metastasis was positively correlated to the expression level of COX-2.

In fact, in the process of tumor hematogenous metastasis, platelets are recognized as the first host cells that tumor cells encounter.[25] To determine the effects of platelets on the hematogenous metastasis of breast cancer, we firstly established a platelet-tumor cell co-incubation system *in vivo*. Intriguingly, it was demonstrated that the 4T1 tumor-bearing mice receiving platelets exhibited aggravated lung metastasis on both day 10 and 20 following cell injection compared with the 4T1 tumor-bearing mice, as shown in the IVIS images (Figures 1E and 1F). Meanwhile, H&E staining results revealed that more lung metastatic nodules in the 4T1 tumor-bearing mice receiving platelets were observed compared with that in the 4T1 tumor-bearing mice (Figures 1G and 1H). Ki67 IHC data also showed that the 4T1 tumor-bearing mice receiving platelets exhibited elevated proliferative abilities compared with 4T1-tumor bearing mice (Figures 1G–1I). To further examine the role of COX-2 in the 4T1 breast cancer cells, we constructed three COX-2 knockout plasmids and selected COX-2-i2 to deplete the expression of COX-2 based on the knockout efficiency (Figures S1A and S1B). More importantly, it was revealed that the COX-2 expression was significantly diminished in the lung metastatic nodules in the mice with COX-2 knocked out 4T1 cells than that in the mice with control 4T1 cells in the presence of platelets (Figures 1M and 1P), and the degree of platelets promoting tumor metastasis was reduced (Figures 1J–1L, 1O, and S1C–S1F). Additionally, we detected the amounts of CTCs isolated from the whole blood of 4T1 tumor-bearing mice in the control and COX-2 knockout group. Intriguingly, the quantification of bioluminescence intensity for CTCs illustrated that the deficiency of COX-2 resulted in profound decrease in the bioluminescence intensity compared with control, indicating that the amounts of CTCs were dramatically mitigated in the absence of COX-2 (Figures 1N and 1Q). Likewise, the expression levels of multiple critical inflammatory cytokines including interleukin (IL)-1β, IL-6 and tumor necrosis factor (TNF)-α in the serum were significantly decreased in the COX-2 knockout group (Figures S1G–S1I). In conclusion, our data suggested that platelets promoted hematogenous metastasis of breast cancer in a COX-2-dependent manner.

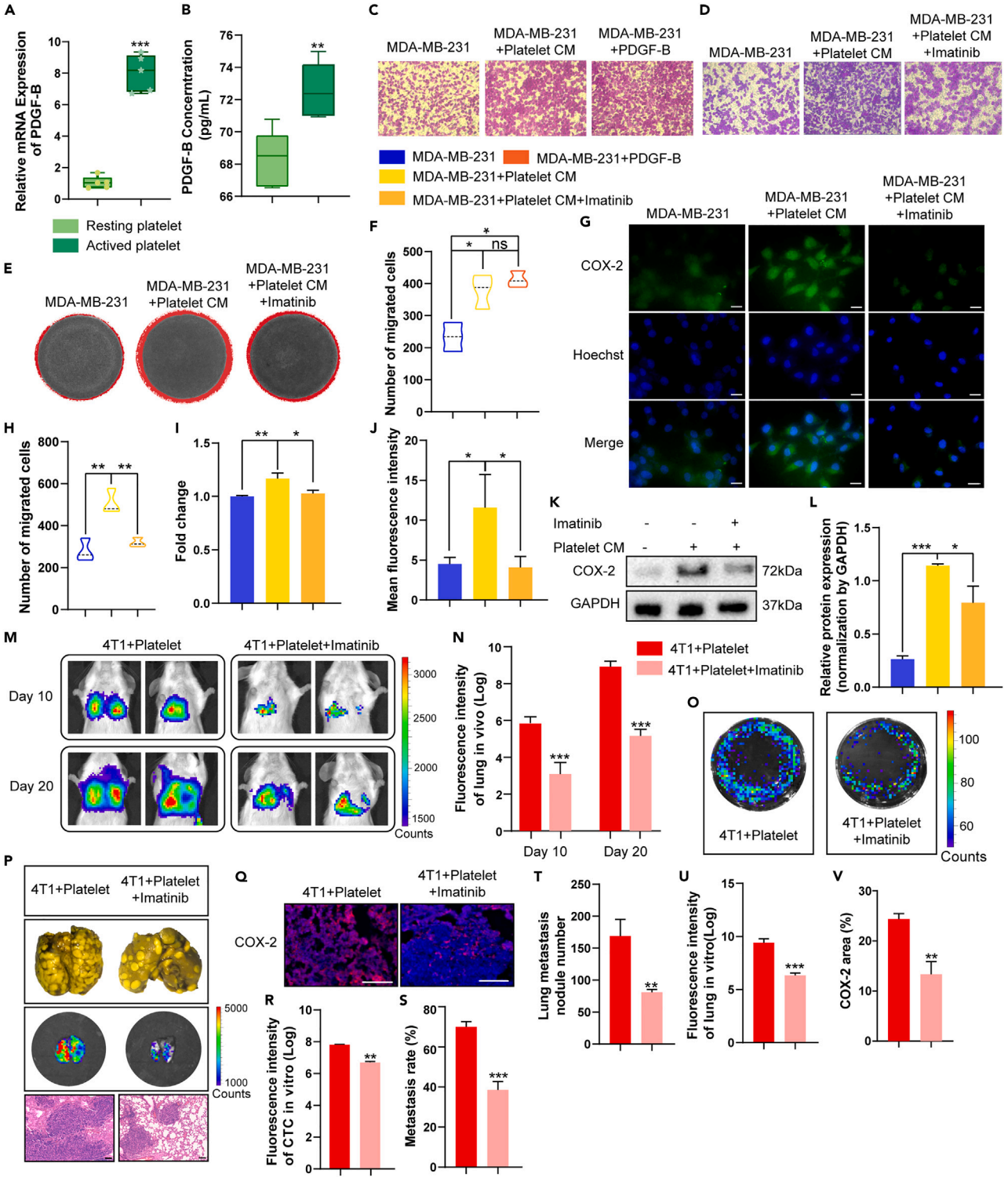

Figure 2. PDGF-B is involved in the activation of platelets and influences COX-2 expression in breast cancer cells

(A) The mRNA expression levels of PDGF-B in the resting and activated platelets (n = 5).

(B) The secretion of PDGF-B in both resting and activated platelets was determined by ELISA (n = 6).

(C) The migration of MDA-MB-231 cells in the presence of CM from activated platelets or PDGF-B was determined by transwell migration assay.

Figure 2. *Continued*

(D) The migration of MDA-MB-231 cells in the presence of CM from activated platelets following the treatment of vehicle control or imatinib was determined by transwell migration assay.

(E) The invasion of MDA-MB-231 cells induced by CM from activated platelets was determined by 3D tumor sphere invasion assay.

(F) Quantification of the migrated MDA-MB-231 cells (n = 6).

(G) Representative immunofluorescence images for COX-2 (green) in the MDA-MB-231 cells induced by CM from platelets.

(H) Quantification of the migrated MDA-MB-231 cells treated with vehicle control or imatinib (n = 6).

(I) Quantification of the 3D tumor sphere invasion assay (n = 6).

(J) Quantification of immunofluorescence for MDA-MB-231 cells (n = 6).

(K) The expression level of COX-2 in the MDA-MB-231 lysates was measured by Western blot analysis. GAPDH was used as a loading control.

(L) Densitometric ratio for the expression level of COX-2 was quantified (n = 3).

(M) Representative bioluminescent images of metastasis in the 4T1-platelet mice treated with saline or imatinib.

(N) Quantification of the bioluminescence imaging signals of the lung metastasis (n = 5).

(O) Representative bioluminescent images of luciferase-positive CTC colonies isolated from the whole blood of 4T1-platelet mice.

(P) Representative images of the nodules on the lung surface, bioluminescent images of metastasis in the harvested lungs and H&E staining of lung tissues in the 4T1-platelet mice.

(Q) Representative images for COX-2 staining (red) in the lung tissue sections of 4T1-platelet mice.

(R) Quantification for the bioluminescence of luciferase-positive CTC colonies (n = 5).

(S) Metastatic rates of 4T1-platelet mice (n = 5).

(T) Quantitative analysis of the number of lung metastatic nodules (n = 5).

(U) Quantification of the bioluminescence imaging signals of the harvested lungs (n = 5).

(V) Quantification of COX-2 positive fields in the lung nodules of mice (n = 4–6).

Data are presented as Mean ± SD. *p < 0.05, **p < 0.01, ***p < 0.001.

PDGF-B is involved in the activation of platelets and influences COX-2 expression in breast cancer cells

Given the fact that we demonstrated that platelets were essential for accelerating the hematogenous metastasis of breast cancer, we intended to further investigate the specific roles of platelets in controlling the progression of breast cancer. To this end, the optimal co-incubation ratio of conditioned medium (CM) from platelets and breast cancer cells was determined accordingly, and it was found that the co-incubation ratio at1:200 contributed to the strongest tumor cell survival ability (Figures S2A and S2B). Furthermore, the mRNA expression levels of VEGF-A, TGF-β and PDGF-B in the platelets were detected, and it was surprisingly observed that the mRNA expression of PDGF-B in the activated platelets was significantly higher than that in the resting platelets (Figures S2C, S2D, and 2A). In line with this, the ELISA results illustrated that the protein level of secreted PDGF-B from activated platelets was markedly increased compared with that from resting platelets (Figure 2B). We further added exogenous PDGF-B or CM from the activated platelet to interfere with cancer cells, the concentration of which was approximately equivalent to that of platelet secretion. Intriguingly, our data revealed that both the CM from activated platelet and PDGF-B substantially enhanced the proliferation and migration of breast cancer cells, as compared to the control group (Figures 2C–2F and S2E–S2L). Next, we explored the effect of PDGFR-β on COX-2 expression induced by CM from platelets. It was demonstrated that imatinib, a classic PDGFR-β inhibitor, suppressed the migration (Figures 2D–2H, S2M, and S2N) and invasion (Figures 2E and 2I) of breast cancer cells, as well as reversed the elevated expression of COX-2 that was mediated by the CM from platelets (Figures 2G and 2J–2L). More interestingly, IVIS results showed that imatinib strikingly attenuated the lung metastasis of breast cancer in the co-incubation system (Figures 2M and 2N), which was substantiated by that the number and area of lung metastatic nodules were significantly reduced following the treatment of imatinib (Figure 2P and 2S–2U). In agreement with this, the expression level of Ki67 was prominently diminished (Figures S2O and S2P) and the number of CTCs was dramatically mitigated (Figures 2O–2R). Immunofluorescence staining showed that imatinib remarkably decreased the expression of COX-2 in the lung metastatic nodules of co-incubated mice (Figures 2Q–2V). Collectively, our data implied that CM from the activated platelets released PDGF-B that acted on the breast cancer cells, driving the distant metastasis of breast cancer cells.

CD36 is responsible for paracrine activation of platelets mediated by breast cancer cells

In order to further dissect the underlying mechanisms of platelet activation, we thus examined the effect of CM from breast cancer cells on activating platelets. It has been widely held that CD36 as a scavenger receptor plays a pivotal role in triggering the activation of platelets.[26,27] Notably, it was elucidated that the CM from MDA-MB-231 cells markedly boosted the expression level of CD36 in the platelets (Figures 3C and 3D). In addition, flow cytometry results illustrated that the CM from MDA-MB-231 cells significantly enhanced the expression of CD62P in the platelets (Figures 3A and 3B), indicating that platelets were activated upon the stimulation of CM from breast cancer cells. These results were consistent with what we observed in the 4T1 cells (Figures S3A–S3D). More interestingly, it was noted that the CM from breast cancer cells was also able to result in the morphological change of platelets (Figures 3G and S3E), as well as escalate platelet adhesion (Figures 3E and 3H) and aggregation functions (Figures 3F–3I). Furthermore, we also found that the erythrocyte sedimentation rate (ESR) was dramatically increased (Figure 3J), and the four types of classic coagulation indexes were changed accordingly in the presence of CM from breast cancer cells (Figures 3K–3N). Taken together, these data suggested that the CM from breast cancer cells stimulated the activation of platelets, culminated the expression level of CD36 in the platelet, and transformed CD36-associated functions.

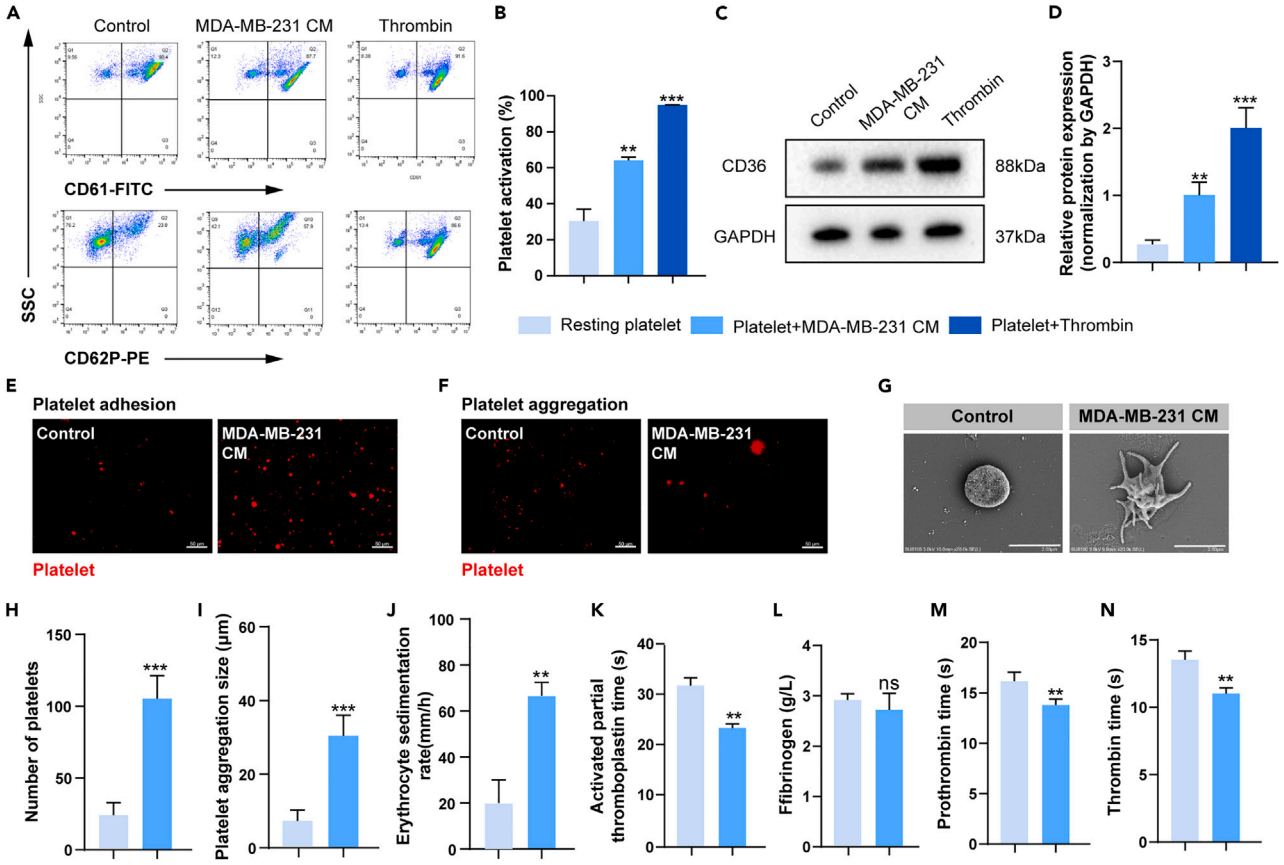

Figure 3. CD36 is responsible for paracrine activation of platelets mediated by breast cancer cells

(A) Flow cytometry analysis of $CD61^{+}CD62P^{+}$ platelets from the healthy volunteers that were activated by the CM from MDA-MB-231 cells and thrombin.

(B) Quantification of flow cytometry analysis for $CD62P^{+}$ platelets (n = 5).

(C) The protein expression level of CD36 in the platelet lysates was measured by Western blot analysis. GAPDH was used as a loading control.

(D) Densitometric ratio for the expression level of CD36 was quantified (n = 3).

(E and F) The abilities of platelet adhesion (E) and aggregation (F) activated by the CM from MDA-MB-231 cells were detected by immunofluorescence assay.

(G) Representative SEM images of the resting and activated platelets from the healthy volunteers (n = 5).

(H and I) Quantification of multiple assays for assessing the platelet adhesion (H) and aggregation (I) functions (n = 6).

(J) Quantification of the effects of resting and activated platelets on ESR index (n = 5).

(K–N) Quantification of the effects of resting and activated platelets on four types of coagulation parameters (n = 5).

Data are presented as Mean ± SD. *p < 0.05, **p < 0.01, ***p < 0.001.

Inhibition of CD36 reverses platelet activation induced by breast cancer cells

Since it has been well recognized that the high expression of CD36 is essential for mediating the activation of platelets,[28] Sal B as a potent inhibitor of CD36[29] was used to determine the role of CD36 inhibition in platelet activation induced by breast cancer cells. Of note, our data showed that 32 μM Sal B prominently eliminated the expression of CD36 expression (Figures 4A and 4B). More intriguingly, it was observed that the mRNA expression of PDGF-B in the platelets was drastically diminished and the release of PDGF-B from the activated platelets was curtailed (Figures 4C and 4D), while the mRNA expression levels of TGF-β and VEGF-A stayed unchanged following the treatment of Sal B (Figures S4A and S4B). On the basis of the flow cytometry analysis, it was demonstrated that inhibition of CD36 strikingly hampered the expression of CD62P, a well-known platelet activation-associated protein (Figures 4E and 4F). SEM data uncovered that Sal B inhibited the morphology and aggregation of activated platelets (Figures 4G, 4H, 4N, and 4O). Moreover, immunofluorescence results manifested that the aggregation and adhesion of platelets could be restricted in the presence of Sal B (Figures 4I, 4J, 4P, and 4Q). The results of clot retraction test elucidated that the aggregation ability of platelets was remarkably suppressed upon Sal B treatment (Figures 4K–4M). Inhibition of CD36 turned down the ESR and reinforced the values of four types of coagulation parameters (Figures S4C–S4G). Consequently, our data implied that inhibition of CD36 blocked the activation of platelets, thereby altering the morphology and function of platelets.

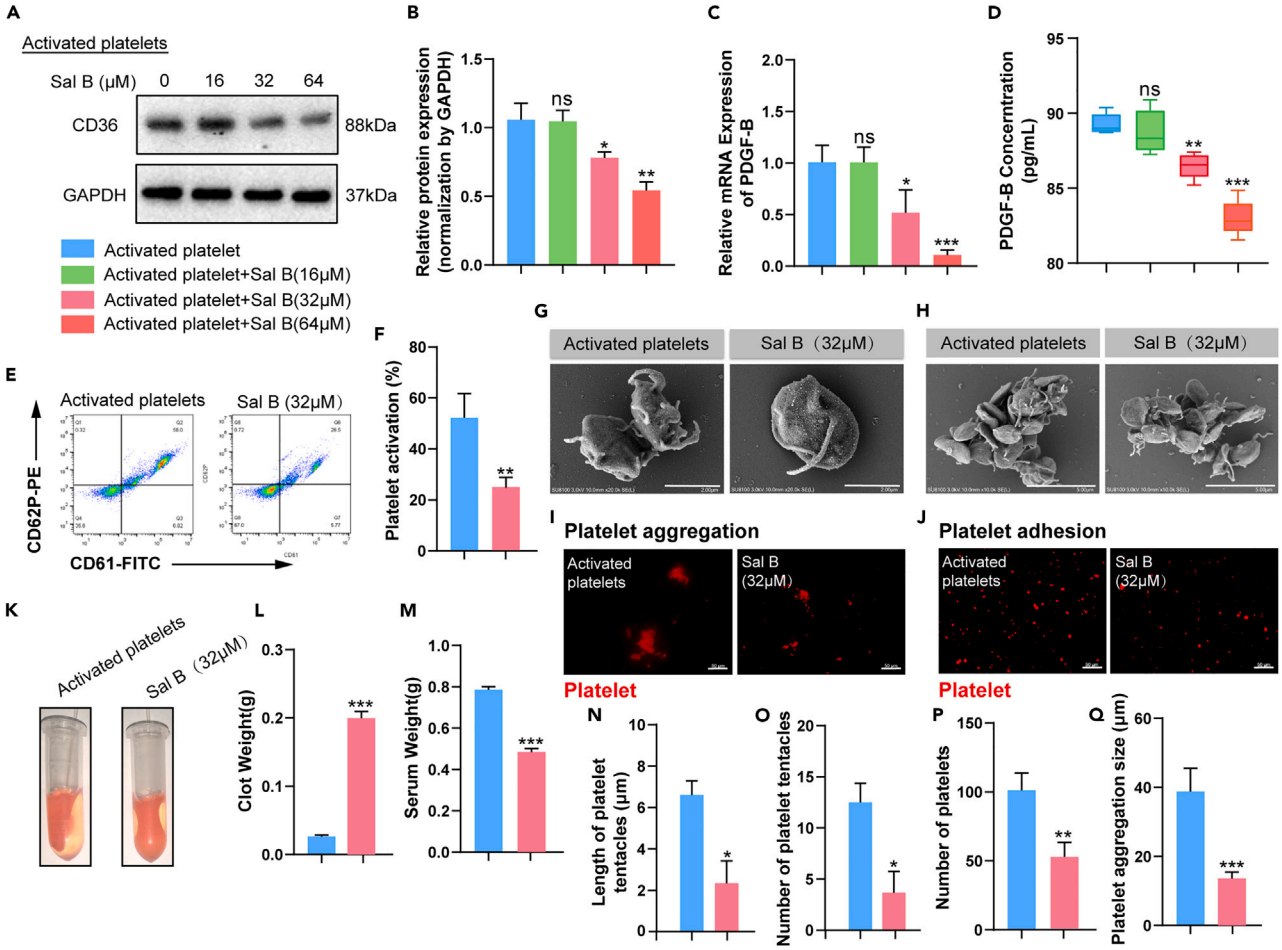

Figure 4. Inhibition of CD36 reverses platelet activation induced by breast cancer cells

(A) The protein expression of CD36 in the activated platelets treated by vehicle control or Sal B was examined by Western blot analysis. GAPDH was used as a loading control.

(B) Densitometric ratios for the expression of CD36 in the lysates from activated platelets were quantified (n = 3).

(C) The mRNA expression level of PDGF-B in the activated platelets treated with vehicle control or Sal B (n = 5).

(D) The level of secreted PDGF-B in the vehicle control or Sal B treated platelets was measured by ELISA (n = 6).

(E) Flow cytometry analysis of $CD61^{+}CD62P^{+}$ activated platelets.

(F) Quantification of flow cytometry analysis for $CD62P^{+}$ platelets (n = 5).

(G and H) Representative SEM images of the morphology (G) and aggregation (H) of activated platelets.

(I and J) The adhesion (I) and aggregation (J) abilities of activated platelets were detected by immunofluorescence assay.

(K) The aggregation function of activated platelets was evaluated by clot retraction assay.

(L and M) Quantitative of the clot retraction assay (L) and serum weight (M) (n = 5).

(N and O) Quantification of the length of platelet tentacles (N) and number of platelet tentacles (O) (n = 5).

(P and Q) Quantification of platelet adhesion (P) and aggregation (Q) (n = 6).

Data are presented as Mean ± SD. *p < 0.05, **p < 0.01, ***p < 0.001.

Restoration of resting platelets inhibited hematogenous metastasis of breast cancer

Given that activated platelets exerted striking impacts on promoting the migration and invasion of breast cancer cells, we further intended to investigate the effects of restoring resting platelets on modulating the hematogenous metastasis of breast cancer. In this regard, Sal B was added into the co-incubation system of platelets and tumor cells. It was illustrated that Sal B contributed to significant decrease in the migration and invasion of MDA-MB-231 cells compared to vehicle control (Figures 5A, 5B, and S5A–S5D). More importantly, when the MDA-MB-231 cells were treated with CM from platelets, they exhibited a spindle-like shape, which was speculated to undergo epithelial-mesenchymal transition (EMT) to increase the metastatic ability of MDA-MB-231 cells (Figure S5H). In line with this, the CM from platelets boosted the expression of N-cadherin but diminished the expression of E-cadherin in the MDA-MB-231 cells (Figures S5E–S5G), which could be reversed in the presence of Sal B and thus inhibited the EMT of MDA-MB-231 cells (Figures 5C–5E). IF staining results revealed

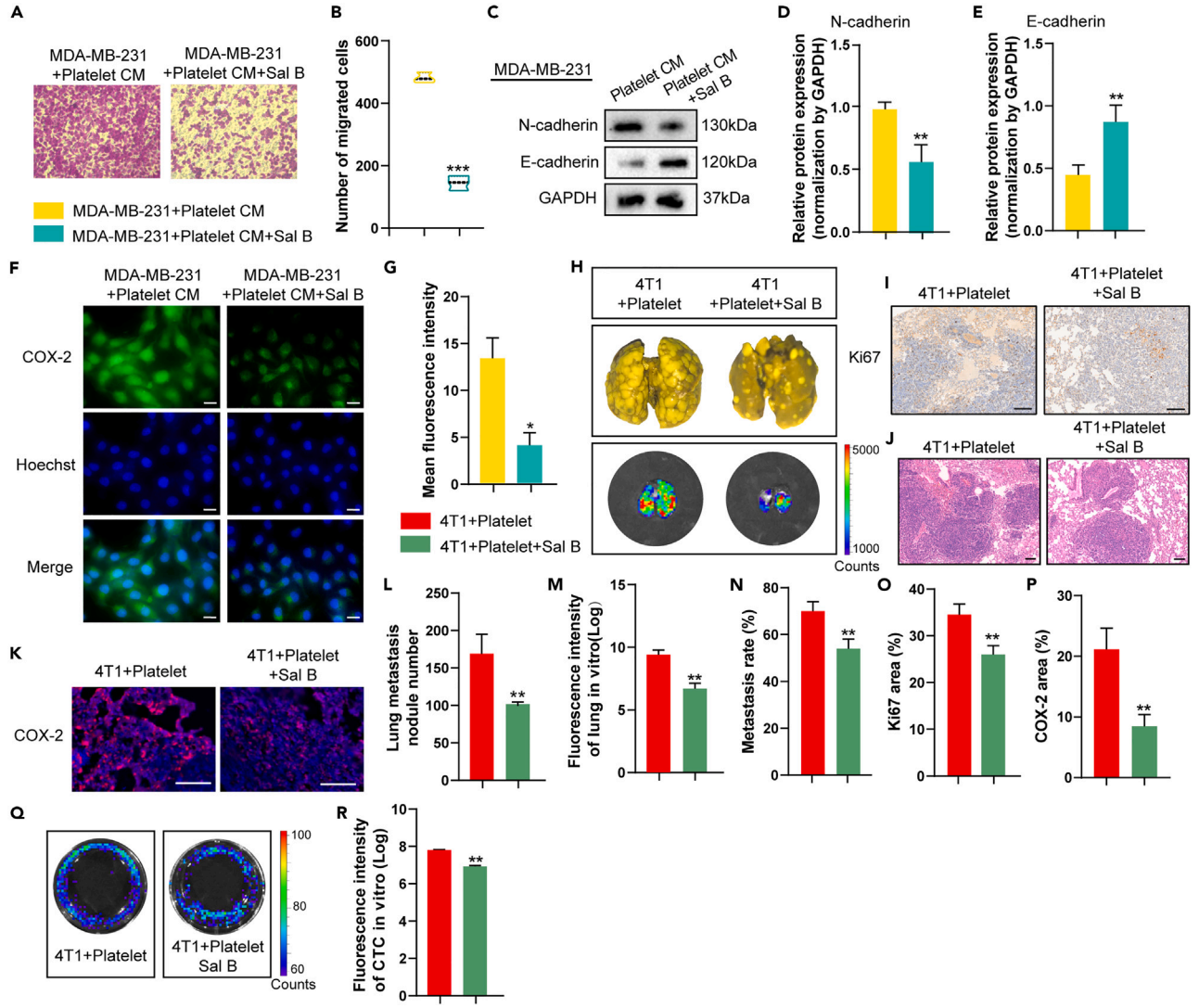

Figure 5. Restoration of resting platelets inhibited hematogenous metastasis of breast cancer

(A) The migration of MDA-MB-231 cells induced by the CM from activated platelets, treated with vehicle control or Sal B, was determined by the transwell migration assay.

(B) Quantification of the migrated MDA-MB-231 cells (n = 6).

(C) The expression levels of N-cadherin and E-cadherin in the MDA-MB-231 cell lysates were measured by Western blot analysis. GAPDH was used as a loading control.

(D and E) Densitometric ratios for the expression levels of N-cadherin (D) and E-cadherin (E) were quantified (n = 3).

(F) Representative immunofluorescence images for COX-2 staining (green) in the MDA-MB-231 cells induced by the CM from activated platelets, treated with vehicle control or Sal B, were shown.

(G) Quantification of COX-2 immunofluorescence in the MDA-MB-231 cells (n = 6).

(H) Representative images for the metastatic nodules on the lung surface and bioluminescent images for metastasis in the harvested lungs of 4T1-platelet mice treated with vehicle control or Sal B.

(I) The IHC staining of Ki67 in the lung tissues in the 4T1-platelet mice, showing the proliferation of tumors.

(J) The H&E staining of lung tissues in the 4T1-platelet mice.

(K) Representative immunofluorescence images of COX-2 (red) in the lung tissue sections of 4T1-platelet mice.

(L) Quantitative analysis of the number of lung metastatic nodules (n = 5).

(M) Quantification of the bioluminescence imaging signals of the harvested lungs (n = 5).

(N) The metastatic rates of 4T1-platelet mice treated with saline or Sal B were quantified (n = 5).

(O) Quantification of the percentage of $Ki67^{+}$ cells in the visual field (n = 5).

Figure 5. *Continued*
(P) Quantification of COX-2 positive fields in in the metastatic nodules of lungs (n = 5).
(Q) Representative bioluminescent images of luciferase-positive CTC colonies isolated from the whole blood of mice.
(R) Quantification for the bioluminescence of luciferase-positive CTC colonies (n = 5).
Data are presented as Mean ± SD. *p < 0.05, **p < 0.01, ***p < 0.001.

that suppression of platelet activation impaired the expression of COX-2 in the MDA-MB-231 cells in the co-culture system (Figures 5F and 5G).

To further validate the impact of platelet activation inhibition on the hematogenous metastasis of breast cancer, Sal B was utilized to intervene the co-incubation system of platelets and tumor cells. It was elucidated that Sal B led to the attenuated platelet-mediated hematogenous metastasis of breast cancer (Figures S5I and S5J). Compared with the vehicle control-treated mice, the tumor burdens in lungs were dramatically reduced in the Sal B-treated mice (Figures 5H, 5J, and 5L–5N). Consistently, the proliferation of 4T1 cells in the lungs, as defined by the Ki67 IHC staining, was observed to be decreased in the Sal B-treated group as compared to the vehicle control-treated group (Figures 5I and 5O). Furthermore, IF staining results uncovered that Sal B prominently decreased the expression of COX-2 expression in the lungs as compared to vehicle control (Figures 5K and 5P). Following the administration of Sal B, the expression levels of TNF-α, IL-6 and IL-1β in the serum were noticeably declined (Figures S5K, S5L, and S5M). Moreover, the bioluminescence analysis of CTCs demonstrated that Sal B treatment resulted in profound decrease in the bioluminescence intensity compared with the treatment of vehicle control (Figures 5Q and 5R), suggesting the amounts of CTCs were dramatically mitigated following the treatment of Sal B. Based on the above-mentioned results, we speculated that inhibition of CD36 with Sal B exerted striking effects on limiting the hematogenous metastasis of breast cancer in the co-culture system, which indicated that restoration of platelets to a resting state is pivotal for restricting metastasis.

CD36 inhibition in combination with celecoxib synergistically suppressed hematogenous metastasis of breast cancer

On the basis of what we observed above, it was concluded that the elevated expression of COX-2 was closely associated with the enhanced hematogenous metastasis of breast cancer in the platelet-tumor microenvironment. Nevertheless, it was increasingly held that celecoxib, a clinically used inhibitor of COX-2, failed to exhibit obvious impact on tumor metastasis *in vivo*.[30,31] To this end, we further examined the effect of Sal B in combination with celecoxib on the hematogenous metastasis of breast cancer in the co-culture system. Interestingly, it was found that the 4T1 tumor-bearing mice treated with Sal B plus celecoxib exhibited fewer metastasis and less tumor burden in lungs compared with the mice treated with celecoxib alone (Figures 6A, 6B, 6H, and 6I). Similarly, the area of tumor and the number of metastatic nodules in lungs following the treatment of Sal B plus celecoxib were strikingly less than those upon the treatment of celecoxib alone (Figures 6B, 6C, 6E, and 6J). Moreover, the combination of Sal B with celecoxib provoked more conspicuous anti-cancer effect as compared to celecoxib alone, as defined by the decreased proliferation of breast cancer cells (Figures 6D and 6K). Additionally, immunofluorescence results unveiled that Sal B in combination with celecoxib gave rise to more prominent decrease in the expression level of COX-2 in the lung tumors (Figures 6G and 6L).

Subsequently, the bioluminescence quantification was performed to analyze the number of CTCs in the blood circulation. It was shown that Sal B in combination with celecoxib remarkably alleviated the bioluminescence intensity, suggesting that the amounts of CTCs were radically curtailed upon combined treatment of Sal B and celecoxib (Figures 6F and 6M). Further, it was uncovered that the expression levels of TNF-α, IL-6 and IL-1β were significantly reduced in the combination treatment group compared with those in the celecoxib treated group (Figures S6A–S6C). Overall, the aforementioned results supported that Sal B in combination with celecoxib alleviated the inflammatory tumor microenvironment by inhibiting COX-2 expression and hampered hematogenous metastasis of breast cancer.

DISCUSSION

In addition to the crucial role in hemostasis maintenance and coagulation after mechanical damage of the blood vessels, platelets have been validated to contain an array of bioactive molecules in their granules. Furthermore, platelets express various receptors on their surfaces that contribute to inflammation, immune suppression, and tumor metastasis.[32,33] Platelets are prone to protect CTCs by encapsulating tumor cells in a thrombus, preventing them from cytolysis by immune cells.[34] Regarding the interactions between platelets and tumor cells, tumor cells can activate platelets via multiple mechanisms, which are also responsible for hypercoagulation and increased thrombosis risks among individuals with cancer. Tumor cells secrete various soluble mediators, including ADP, TXA2, or high-mobility group box 1 (HMGB1), which tend to ligate with toll-like receptor 4 (TLR4) to provoke a local and robust platelet activation.[35–37] In the current research, the collected data supported the hypothesis that breast cancer cells gave rise to platelet activation by secreting distinct inflammatory cytokines. Consequently, the activated platelets released critical factors, including PDGF-B, leading to the increased hematogenous metastasis of breast cancer.

During platelet activation and aggregation, platelets exhibit a preference for secreting a variety of mediators, including multiple crucial pro-inflammatory factors.[38] These factors serve as recruiters and activators of leukocytes, assisting the immune regulative and pro-inflammatory functions of platelets.[39,40] Of note, these multiple platelet-associated functions are crosslinked; activation of platelet inflammatory property contributes to thrombosis, which in various disease conditions tends to lead to worsened or chronic pathogenesis in particular cancer.[41] Herein, it was demonstrated that the activated platelets by the CM from tumor cells were prone to alter morphology and enhanced the adhesion and aggregation function of platelets. Conversely, resting platelets tended to stay suspended without activation. More importantly, activated platelets promoted the migration and invasion of MDA-MB-231 and 4T1 breast cancer cells both *in vitro* and *in vivo*.

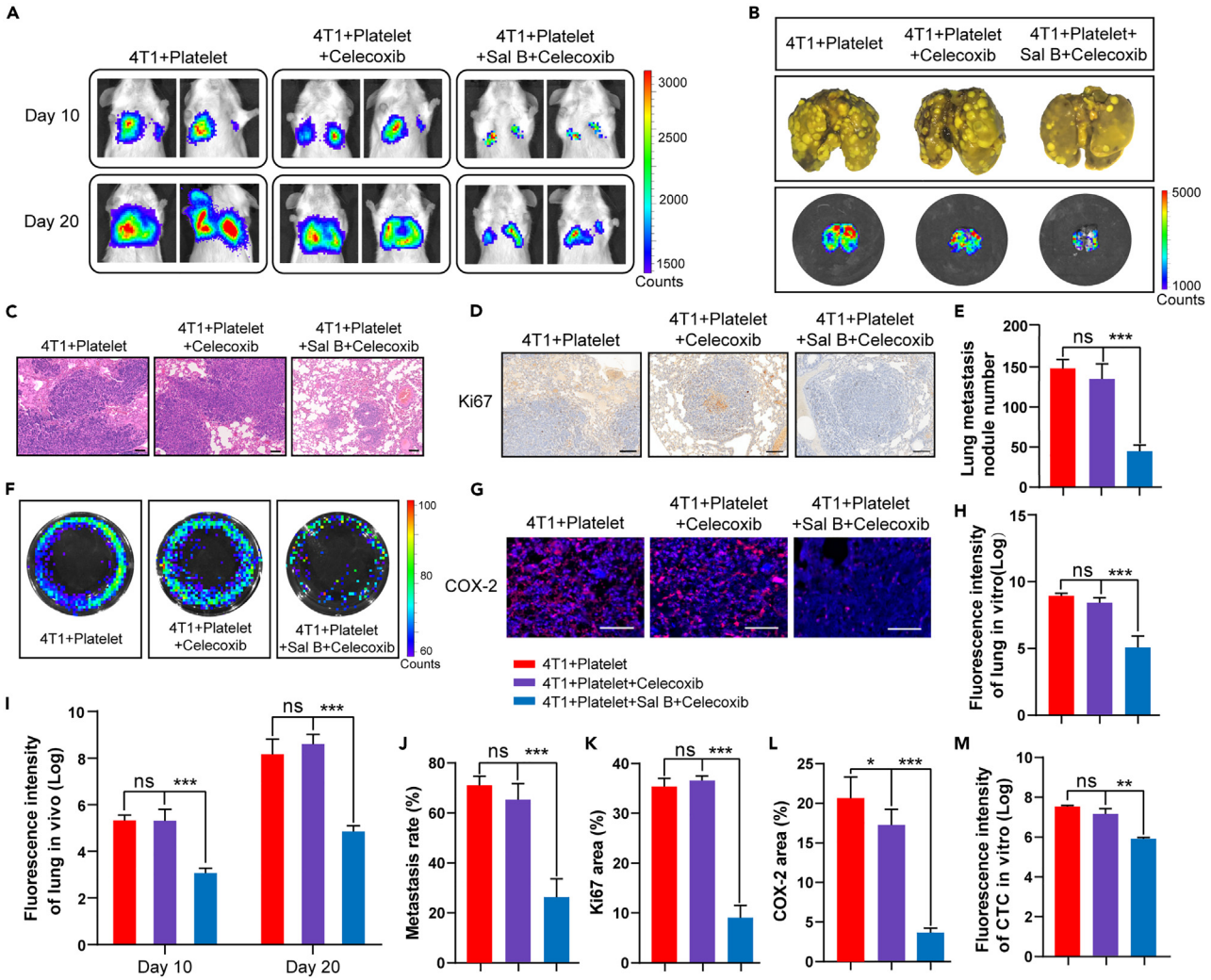

Figure 6. CD36 inhibition in combination with Celecoxib synergistically suppressed hematogenous metastasis of breast cancer

(A) Representative bioluminescent images for the metastasis of the 4T1-platelet mice treated with saline, celecoxib or Sal B plus celecoxib.

(B) Representative images of the metastatic nodules on lung surface and representative bioluminescent images of metastasis in the harvested lungs of 4T1-platelet mice.

(C) The H&E staining for the lung tissues of 4T1-platelet mice.

(D) The IHC staining for Ki67 in the lung tissues of 4T1-platelet mice.

(E) Quantitative analysis for the number of metastatic nodules in lungs(n = 5).

(F) Representative bioluminescent images of luciferase-positive CTC colonies isolated from the whole blood of mice.

(G) Representative images for COX-2 staining (red) in the lung tissue sections of 4T1-platelet mice.

(H) Quantification for the bioluminescence imaging signals of the harvested lungs (n = 5).

(I) Quantification for the bioluminescence imaging signals of the lung metastasis (n = 5).

(J) The metastatic rates of 4T1-platelet mice (n = 5).

(K) Quantification of the percentage of $Ki67^{+}$ cells in the visual field (n = 6).

(L) Quantification of COX-2 positive fields in the metastatic nodules of lungs (n = 5).

(M) Bioluminescence quantification of luciferase-positive CTC colonies (n = 5).

Data are presented as Mean ± SD.*p < 0.05, **p < 0.01, ***p < 0.001.

COX-2, an inducible COX-enzyme isotype, is one of the most crucial inflammatory factors in both acute and chronic pathological states.[42] It is a functional enzyme participating in prostaglandin production under pathological conditions and is highly expressed in precancerous and malignant lesions.[43] COX-2 is deemed a driving force in the progression of tumors owing to its fundamental role in inflammation, angiogenesis, immunosuppression, and invasiveness.[18,44] In the co-culture system of platelets and tumor cells, it was reported that activated platelets boosted the expression of COX-2, further stabilizing cancer cells. This interaction between platelets and tumor cells initiated the secretion of

PGE2 from tumor cells.[45] The data obtained from this study provided compelling evidence that COX-2 upregulation in the breast cancer cells triggered by activated platelets played critical roles in promoting the proliferation, migration, and invasion of breast cancer cells. Of note, the upregulation of COX-2 was found to be correlated with the increased metastasis in breast cancer patients on the basis of GEO database, which is mainly used to explore gene expression in diseases.[46] It was also illustrated that intake of COX-2 inhibitors could regulate a series of events that are associated with progression of breast cancer, including the EMT progress of tumor cells, immune cell infiltration, and chemoresistance,[47–49] and this further supported the rationality for COX-2 inhibitors in combination with other therapies for the treatment of breast cancer.

PDGF-B, a member of the PDGFs family, can bind to its PDGFR-β receptor to promote cell survival, proliferation, and migration.[50] Notably, high expression of both PDGF and PDGFR-β has been validated in multiple human tumor types, such as colon, gastric, lung, pancreatic, and ovarian carcinomas and glioblastomas.[51,52] It was documented that PDGF-B exerted a paracrine effect on the proliferation of benign and malignant breast epithelial cells and, thus, lymphatic metastasis.[53] Consistent with these studies, the findings of this research supported the notion that PDGF-B, released by activated platelets, interacted with PDGFR-β in breast cancer cells. This interaction led to an increased expression level of COX-2 within the breast cancer cells, ultimately facilitating the migration and invasion of these cells and contributing to distal metastasis.

Sal B, a key component of *Salvia miltiorrhiza* Burge, has been extensively studied and proven to possess considerable anti-inflammatory and anti-oxidative effects on various malignant and cardiovascular diseases.[54] However, the potential of Sal B to regulate platelet activation and its impact on the growth of breast cancer is yet to be elucidated. On the basis of relevant literature, Sal B was able to inhibit the expression of CD36, a key factor inducing platelet activation, in the fibroblasts.[29] This research showed that Sal B acted as a CD36 inhibitor and exerted an inhibitory effect on activating platelets. It was further illustrated that Sal B tended to suppress the level of PDGF-B released by activated platelets by diminishing the expression of CD36 in the platelets. In the platelet and tumor cell co-culture system, the reduced PDGF-B level from activated platelets influenced the PDGFR-β/COX-2 axis-associated inflammatory signaling pathways on breast cancer cells. This reduction also mitigated the expression of COX-2 and thus delayed the progression of tumor metastasis mediated by activated platelets.

Celecoxib is a nonsteroidal anti-inflammatory drug (NSAID) designed to selectively target COX-2.[55] It was reported that celecoxib decreased TNF-α, G-CSF, and IL-6 levels in tumor-bearing mice.[56] However, celecoxib treatment alone failed to influence tumor metastasis.[30] Consistently, this study elucidated that celecoxib slightly alleviated the expression of COX-2 and the levels of various serum inflammatory cytokines, including IL-6, IL-1β, and TNF-α in the mice with hematogenous metastasis of breast cancer. However, there was no significant variation in light of tumor metastasis between platelet and celecoxib-treated groups. Nevertheless, the combination of celecoxib with Sal B exhibited a significant enhancement in the effect of inhibiting tumor metastasis. Based on these findings, it is reasonable to speculate that anti-platelet therapy has the potential to become an effective adjuvant therapy for preventing tumor recurrence and metastasis in a clinical setting. Currently, anti-platelet drugs still fail to become routine pharmacological cancer prevention and treatment strategies. The utilization of anti-platelet drugs for cancer prevention and treatment means long-term administration, which ultimately elevates the risk of bleeding.[57,58] Another potential clinical scenario where the benefit-to-risk ratio may be favorable is using anti-platelet drugs as short-term adjuvants for radiotherapy or surgery. It is important to highlight that recent clinical trials serve as reminders of the existing challenges in the field. These challenges include the development of safe anti-platelet strategies aimed at improving treatment outcomes for cancer patients and gaining a deeper understanding of the complex mechanisms underlying pathological processes induced by platelets.

In conclusion, our findings demonstrated that the expression of COX-2 in breast cancer patients was closely related to the degree of metastasis. *In vivo* experimental evidence revealed that co-incubation of platelets with breast cancer cells significantly improved the lung metastasis of breast cancer. Under the circumstance of platelets interacting with breast cancer cells, the enhanced expression level of CD36 resulted in the activation of platelets, thereby contributing to the elevated secretion of PDGF-B in the inflammatory tumor microenvironment. Additionally, PDGF-B was prone to interact with PDGFR-β to boost the expression of COX-2 in the breast cancer cells, thus aggravating the progression of metastasis. Blockade of CD36 on the activated platelets in combination with celecoxib synergistically diminished the expression of COX-2 and prevented platelet-driven distant metastasis. Given that tumor combination therapy is gaining increasing attention in clinical practice, this study may provide new avenues to improve clinical outcomes for individuals with breast cancer.

Limitations of the study

Although our study provided strong evidence that the linkage between CD36 and COX-2 participated in the interactions between platelets and breast cancer cells, promoting the metastasis of breast cancer, as well as co-inhibition of CD36 and COX-2 could remarkedly synergize against breast cancer metastasis, there were still some unanswered questions that warrant further exploration. First, considering that the COX-2 inhibitor celecoxib failed to significantly inhibit tumor metastasis in clinic trial, we explored the effect of CD36 inhibitor Sal B in combination with celecoxib on influencing breast cancer metastasis. However, we did not investigate whether co-inhibition of PDGFR-β and CD36 could also play a synergistic role in restricting metastasis of breast cancer. Furthermore, we evaluated the interaction mechanisms between platelets and breast cancer, but did not extend to other cancer types, and we only verified it in the tail-vein injection model of breast cancer metastasis. In future studies, we plan to explore the role of CD36 in the platelets and COX-2 in the tumor cells in the *in- situ* model and other cancer types. Finally, as mentioned in the Discussion part, recent studies reported that the combination of COX-2 inhibitors aspirin or celecoxib with chemotherapy agents, anti-angiogenic drugs, and immune checkpoint inhibitors exerted significant synergistic anti-cancer effects. This suggested that we should also consider the influence on the composition of immune cells and angiogenesis in the tumor microenvironment from the discovered interactions between platelets and cancer cells, which is worthy of in-depth exploration in future study.

STAR★METHODS

Detailed methods are provided in the online version of this paper and include the following:

- KEY RESOURCES TABLE
- RESOURCE AVAILABILITY
  - Lead contact
  - Materials availability
  - Data and code availability
- EXPERIMENTAL MODEL AND STUDY PARTICIPANT DETAILS
  - Study approval
  - Animals
- METHOD DETAILS
  - Cell culture
  - Patient samples
  - Plasmid transfection
  - Platelet isolation
  - CCK8 assay
  - Enzyme-linked immunosorbent assay (ELISA)
  - Wound healing and transwell migration assays
  - Western blotting
  - Co-culture system
  - Clot retraction assay
  - Platelet adhesion and aggregation assays
  - Hemocyte sedimentation and coagulation index examination
  - Quantitative RT-PCR
  - Flow cytometry
  - Scanning electron microscopy (SEM)
  - IHC staining
  - IF staining
  - H&E staining
  - Bioluminescence imaging for tumor monitoring
  - Detection of circulating tumor cells (CTCs)
  - Bioinformatics analysis
- QUANTIFICATION AND STATISTICAL ANALYSIS
  - Statistical analysis

SUPPLEMENTAL INFORMATION

Supplemental information can be found online at https://doi.org/10.1016/j.isci.2023.107704.

ACKNOWLEDGMENTS

We thank resources provided by the Experiment Center for Science and Technology in Nanjing University of Chinese Medicine. We are grateful to our laboratory companions for their assistance in this work.

This work was financially supported by the projects of National Natural Science Foundation of China (81973587 to A.W.; 82003991 to Y. Z.; 81973734 to Y. L.); Jiangsu Specially Appointed Professorship Foundation (013038021001 to Y. Z.); Jiangsu Province Traditional Chinese Medicine Leading Talents Program (SLJ0229 to Y. L.); The Postgraduate Research & Practice Innovation Program of Jiangsu Province (SJCX22-0791 to Y. T.; KYCX22-2045 to C. Q.).

AUTHOR CONTRIBUTIONS

A.W., Y. Z., and Y. L. designed and led the project. Y. T. and C. Q. conducted most experiments. Y. Z. conducted some experiments related to mice and cell culture. C. Y. made contributions to platelet collection. M. S. and T.Z. performed IHC staining and flow cytometer. X. M. conducted clinical study and analyzed the data. Y. T. and C. Q. prepared the preliminary paper and contributed equally to this work. Y. Z. revised and rewrote the paper. All authors have read and approved the final manuscript.

DECLARATION OF INTERESTS

The authors declare that they have no competing interest that could have appeared to influence the work reported in this paper.

INCLUSION AND DIVERSITY

We support inclusive, diverse, and equitable conduct of research.

Received: May 24, 2023
Revised: July 3, 2023
Accepted: August 21, 2023
Published: August 23, 2023

REFERENCES

1. Lin, Y., Xu, J., and Lan, H. (2019). Tumor-associated macrophages in tumor metastasis: biological roles and clinical therapeutic applications. J. Hematol. Oncol. *12*, 76. https://doi.org/10.1186/s13045-019-0760-3.
2. Sabrkhany, S., Kuijpers, M.J.E., Griffioen, A.W., and Oude Egbrink, M.G.A. (2019). Platelets: the holy grail in cancer blood biomarker research? Angiogenesis *22*, 1–2. https://doi.org/10.1007/s10456-018-9651-4.
3. Franco, A.T., Corken, A., and Ware, J. (2015). Platelets at the interface of thrombosis, inflammation, and cancer. Blood *126*, 582–588. https://doi.org/10.1182/blood-2014-08-531582.
4. Haemmerle, M., Stone, R.L., Menter, D.G., Afshar-Kharghan, V., and Sood, A.K. (2018). The Platelet Lifeline to Cancer: Challenges and Opportunities. Cancer Cell *33*, 965–983. https://doi.org/10.1016/j.ccell.2018.03.002.
5. Ward, Y., Lake, R., Faraji, F., Sperger, J., Martin, P., Gilliard, C., Ku, K.P., Rodems, T., Niles, D., Tillman, H., et al. (2018). Platelets Promote Metastasis via Binding Tumor CD97 Leading to Bidirectional Signaling that Coordinates Transendothelial Migration. Cell Rep. *23*, 808–822. https://doi.org/10.1016/j.celrep.2018.03.092.
6. Koupenova, M., Clancy, L., Corkrey, H.A., and Freedman, J.E. (2018). Circulating Platelets as Mediators of Immunity, Inflammation, and Thrombosis. Circ. Res. *122*, 337–351. https://doi.org/10.1161/CIRCRESAHA.117.310795.
7. Leblanc, R., Houssin, A., and Peyruchaud, O. (2018). Platelets, autotaxin and lysophosphatidic acid signalling: win-win factors for cancer metastasis. Br. J. Pharmacol. *175*, 3100–3110. https://doi.org/10.1111/bph.14362.
8. Wen, Y.H., and Chen, D.P. (2018). Human platelet antigens in disease. Clin. Chim. Acta *484*, 87–90. https://doi.org/10.1016/j.cca.2018.05.009.
9. Yeh, J.J., Tsai, S., Wu, D.C., Wu, J.Y., Liu, T.C., and Chen, A. (2010). P-selectin-dependent platelet aggregation and apoptosis may explain the decrease in platelet count during Helicobacter pylori infection. Blood *115*, 4247–4253. https://doi.org/10.1182/blood-2009-09-241166.
10. Meikle, C.K.S., Kelly, C.A., Garg, P., Wuescher, L.M., Ali, R.A., and Worth, R.G. (2016). Cancer and Thrombosis: The Platelet Perspective. Front. Cell Dev. Biol. *4*, 147. https://doi.org/10.3389/fcell.2016.00147.
11. Van de Werf, F. (2011). Inhibitors of the platelet thrombin receptor: will they live up to their promises? Circulation *123*, 1833–1835. https://doi.org/10.1161/CIRCULATIONAHA.111.021733.
12. Campanella, R., Guarnaccia, L., Cordiglieri, C., Trombetta, E., Caroli, M., Carrabba, G., La Verde, N., Rampini, P., Gaudino, C., Costa, A., et al. (2020). Tumor-Educated Platelets and Angiogenesis in Glioblastoma: Another Brick in the Wall for Novel Prognostic and Targetable Biomarkers, Changing the Vision from a Localized Tumor to a Systemic Pathology. Cells *9*. https://doi.org/10.3390/cells9020294.
13. López, D.E., and Ballaz, S.J. (2020). The Role of Brain Cyclooxygenase-2 (Cox-2) Beyond Neuroinflammation: Neuronal Homeostasis in Memory and Anxiety. Mol. Neurobiol. *57*, 5167–5176. https://doi.org/10.1007/s12035-020-02087-x.
14. Dhir, A. (2019). An update of cyclooxygenase (COX)-inhibitors in epilepsy disorders. Expert Opin. Investig. Drugs *28*, 191–205. https://doi.org/10.1080/13543784.2019.1557147.
15. Gupta, S.C., Kunnumakkara, A.B., Aggarwal, S., and Aggarwal, B.B. (2018). Inflammation, a Double-Edge Sword for Cancer and Other Age-Related Diseases. Front. Immunol. *9*, 2160. https://doi.org/10.3389/fimmu.2018.02160.
16. Yao, C., and Narumiya, S. (2019). Prostaglandin-cytokine crosstalk in chronic inflammation. Br. J. Pharmacol. *176*, 337–354. https://doi.org/10.1111/bph.14530.
17. Wang, D., and Dubois, R.N. (2010). The role of COX-2 in intestinal inflammation and colorectal cancer. Oncogene *29*, 781–788. https://doi.org/10.1038/onc.2009.421.
18. Simonsson, M., Björner, S., Markkula, A., Nodin, B., Jirström, K., Rose, C., Borgquist, S., Ingvar, C., and Jernström, H. (2017). The prognostic impact of COX-2 expression in breast cancer depends on oral contraceptive history, preoperative NSAID use, and tumor size. Int. J. Cancer *140*, 163–175. https://doi.org/10.1002/ijc.30432.
19. Mammadova-Bach, E., Gil-Pulido, J., Sarukhanyan, E., Burkard, P., Shityakov, S., Schonhart, C., Stegner, D., Remer, K., Nurden, P., Nurden, A.T., et al. (2020). Platelet glycoprotein VI promotes metastasis through interaction with cancer cell-derived galectin-3. Blood *135*, 1146–1160. https://doi.org/10.1182/blood.2019002649.
20. Cimmino, G., Tarallo, R., Nassa, G., De Filippo, M.R., Giurato, G., Ravo, M., Rizzo, F., Conte, S., Pellegrino, G., Cirillo, P., et al. (2015). Activating stimuli induce platelet microRNA modulation and proteome reorganisation. Thromb. Haemostasis *114*, 96–108. https://doi.org/10.1160/TH14-09-0726.
21. Colkesen, Y., and Muderrisoglu, H. (2012). The role of mean platelet volume in predicting thrombotic events. Clin. Chem. Lab. Med. *50*, 631–634. https://doi.org/10.1515/CCLM.2011.806.
22. Shu, H., Peng, Y., Hang, W., Nie, J., Zhou, N., and Wang, D.W. (2022). The role of CD36 in cardiovascular disease. Cardiovasc. Res. *118*, 115–129. https://doi.org/10.1093/cvr/cvaa319.
23. Qi, Z., Hu, L., Zhang, J., Yang, W., Liu, X., Jia, D., Yao, Z., Chang, L., Pan, G., Zhong, H., et al. (2021). PCSK9 (Proprotein Convertase Subtilisin/Kexin 9) Enhances Platelet Activation, Thrombosis, and Myocardial Infarct Expansion by Binding to Platelet CD36. Circulation *143*, 45–61. https://doi.org/10.1161/CIRCULATIONAHA.120.046290.
24. Tang, Y., Guo, H., Chen, L., Wang, X., Chen, Q., Gou, L., Liu, X., and Wang, X. (2023). Development and validation of a prognostic model for mitophagy-related genes in colon adenocarcinoma: A study based on TCGA and GEO databases. PLoS One *18*, e0284089. https://doi.org/10.1371/journal.pone.0284089.
25. Suzuki-Inoue, K. (2019). Platelets and cancer-associated thrombosis: focusing on the platelet activation receptor CLEC-2 and podoplanin. Blood *134*, 1912–1918. https://doi.org/10.1182/blood.2019001388.
26. Park, Y.M. (2014). CD36, a scavenger receptor implicated in atherosclerosis. Exp. Mol. Med. *46*, e99. https://doi.org/10.1038/emm.2014.38.
27. Yang, M., and Silverstein, R.L. (2019). CD36 and ERK5 link dyslipidemia to apoptotic-like platelet procoagulant function. Curr. Opin. Hematol. *26*, 357–365. https://doi.org/10.1097/MOH.0000000000000522.
28. Yang, M., Cooley, B.C., Li, W., Chen, Y., Vasquez-Vivar, J., Scoggins, N.O., Cameron, S.J., Morrell, C.N., and Silverstein, R.L. (2017). Platelet CD36 promotes thrombosis by activating redox sensor ERK5 in hyperlipidemic conditions. Blood *129*, 2917–2927. https://doi.org/10.1182/blood-2016-11-750133.
29. Griffin, M.F., Borrelli, M.R., Garcia, J.T., Januszyk, M., King, M., Lerbs, T., Cui, L., Moore, A.L., Shen, A.H., Mascharak, S., et al. (2021). JUN promotes hypertrophic skin scarring via CD36 in preclinical in vitro and in vivo models. Sci. Transl. Med. *13*, eabb3312. https://doi.org/10.1126/scitranslmed.abb3312.
30. Zhang, G., Panigrahy, D., Hwang, S.H., Yang, J., Mahakian, L.M., Wettersten, H.I., Liu, J.Y., Wang, Y., Ingham, E.S., Tam, S., et al. (2014). Dual inhibition of cyclooxygenase-2 and soluble epoxide hydrolase synergistically suppresses primary tumor growth and metastasis. Proc. Natl. Acad. Sci. USA *111*, 11127–11132. https://doi.org/10.1073/pnas.1410432111.
31. Booth, L., Roberts, J.L., Cruickshanks, N., Tavallai, S., Webb, T., Samuel, P., Conley, A., Binion, B., Young, H.F., Poklepovic, A., et al. (2015). PDE5 inhibitors enhance celecoxib killing in multiple tumor types. J. Cell. Physiol. *230*, 1115–1127. https://doi.org/10.1002/jcp.24843.
32. Delaney, C., Davizon-Castillo, P., Allawzi, A., Posey, J., Gandjeva, A., Neeves, K., Tuder,

R.M., Di Paola, J., Stenmark, K.R., and Nozik, E.S. (2021). Platelet activation contributes to hypoxia-induced inflammation. Am. J. Physiol. Lung Cell Mol. Physiol. *320*, L413–L421. https://doi.org/10.1152/ajplung.00519.2020.

33. Bakogiannis, C., Sachse, M., Stamatelopoulos, K., and Stellos, K. (2019). Platelet-derived chemokines in inflammation and atherosclerosis. Cytokine *122*, 154157. https://doi.org/10.1016/j.cyto.2017.09.013.
34. Bahmani, B., Gong, H., Luk, B.T., Haushalter, K.J., DeTeresa, E., Previti, M., Zhou, J., Gao, W., Bui, J.D., Zhang, L., et al. (2021). Intratumoral immunotherapy using platelet-cloaked nanoparticles enhances antitumor immunity in solid tumors. Nat. Commun. *12*, 1999. https://doi.org/10.1038/s41467-021-22311-z.
35. Ren, J., He, J., Zhang, H., Xia, Y., Hu, Z., Loughran, P., Billiar, T., Huang, H., and Tsung, A. (2021). Platelet TLR4-ERK5 Axis Facilitates NET-Mediated Capturing of Circulating Tumor Cells and Distant Metastasis after Surgical Stress. Cancer Res. *81*, 2373–2385. https://doi.org/10.1158/0008-5472.CAN-20-3222.
36. Xu, X.R., Yousef, G.M., and Ni, H. (2018). Cancer and platelet crosstalk: opportunities and challenges for aspirin and other antiplatelet agents. Blood *131*, 1777–1789. https://doi.org/10.1182/blood-2017-05-743187.
37. Liang, X., Xiu, C., Liu, M., Lin, C., Chen, H., Bao, R., Yang, S., and Yu, J. (2019). Platelet-neutrophil interaction aggravates vascular in fl ammation and promotes the progression of atherosclerosis by activating the TLR4/NF-kappaB pathway. J. Cell. Biochem. *120*, 5612–5619. https://doi.org/10.1002/jcb.27844.
38. Tesfamariam, B. (2016). Involvement of platelets in tumor cell metastasis. Pharmacol. Ther. *157*, 112–119. https://doi.org/10.1016/j.pharmthera.2015.11.005.
39. Herter, J.M., Rossaint, J., and Zarbock, A. (2014). Platelets in inflammation and immunity. J. Thromb. Haemostasis *12*, 1764–1775. https://doi.org/10.1111/jth.12730.
40. Chen, J., and Tan, W. (2020). Platelet activation and immune response in diabetic microangiopathy. Clin. Chim. Acta *507*, 242–247. https://doi.org/10.1016/j.cca.2020.04.042.
41. Geranpayehvaghei, M., Dabirmanesh, B., Khaledi, M., Atabakhshi-Kashi, M., Gao, C., Taleb, M., Zhang, Y., Khajeh, K., and Nie, G. (2021). Cancer-associated-platelet-inspired nanomedicines for cancer therapy. Wiley Interdiscip. Rev. Nanomed. Nanobiotechnol. *13*, e1702. https://doi.org/10.1002/wnan.1702.
42. Wang, X., Chen, J., and Zheng, J. (2023). The roles of COX-2 in protozoan infection. Front. Immunol. *14*, 955616. https://doi.org/10.3389/fimmu.2023.955616.
43. Mahboubi Rabbani, S.M.I., and Zarghi, A. (2019). Selective COX-2 inhibitors as anticancer agents: a patent review (2014-2018). Expert Opin. Ther. Pat. *29*, 407–427. https://doi.org/10.1080/13543776.2019.1623880.
44. Mattsson, J.S.M., Bergman, B., Grinberg, M., Edlund, K., Marincevic, M., Jirström, K., Pontén, F., Hengstler, J.G., Rahnenführer, J., Karlsson, M.G., et al. (2015). Prognostic impact of COX-2 in non-small cell lung cancer: a comprehensive compartment-specific evaluation of tumor and stromal cell expression. Cancer Lett. *356*, 837–845. https://doi.org/10.1016/j.canlet.2014.10.032.
45. Hashemi Goradel, N., Najafi, M., Salehi, E., Farhood, B., and Mortezaee, K. (2019). Cyclooxygenase-2 in cancer: A review. J. Cell. Physiol. *234*, 5683–5699. https://doi.org/10.1002/jcp.27411.
46. Xu, W., Zhang, Z., Yao, L., Xue, B., Xi, H., Wang, X., and Sun, S. (2022). Exploration of Shared Gene Signatures and Molecular Mechanisms Between Periodontitis and Nonalcoholic Fatty Liver Disease. Front. Genet. *13*, 939751. https://doi.org/10.3389/fgene.2022.939751.
47. Bell, C.R., Pelly, V.S., Moeini, A., Chiang, S.C., Flanagan, E., Bromley, C.P., Clark, C., Earnshaw, C.H., Koufaki, M.A., Bonavita, E., and Zelenay, S. (2022). Chemotherapy-induced COX-2 upregulation by cancer cells defines their inflammatory properties and limits the efficacy of chemoimmunotherapy combinations. Nat. Commun. *13*, 2063. https://doi.org/10.1038/s41467-022-29606-9.
48. Song, M., Qian, C., Zhang, T., Tang, Y., Zhou, Y., Wei, Z., Wang, A., Zhong, C., Zhao, Y., and Lu, Y. (2023). Salvia mitiorrhiza Bunge aqueous extract attenuates infiltration of tumor-associated macrophages and potentiates anti-PD-L1 immunotherapy in colorectal cancer through modulating Cox2/PGE2 cascade. J. Ethnopharmacol. *316*, 116735. https://doi.org/10.1016/j.jep.2023.116735.
49. Lala, P.K., Nandi, P., and Majumder, M. (2018). Roles of prostaglandins in tumor-associated lymphangiogenesis with special reference to breast cancer. Cancer Metastasis Rev. *37*, 369–384. https://doi.org/10.1007/s10555-018-9734-0.
50. Zaidi, M., Lizneva, D., and Yuen, T. (2021). The role of PDGF-BB in the bone-vascular relationship during aging. J. Clin. Invest. *131*, e153644. https://doi.org/10.1172/JCI153644.
51. Du, S., Yang, Z., Lu, X., Yousuf, S., Zhao, M., Li, W., Miao, J., Wang, X., Yu, H., Zhu, X., et al. (2021). Anoikis resistant gastric cancer cells promote angiogenesis and peritoneal metastasis through C/EBPbeta-mediated PDGFB autocrine and paracrine signaling. Oncogene *40*, 5764–5779. https://doi.org/10.1038/s41388-021-01988-y.
52. Zhang, Y., Cedervall, J., Hamidi, A., Herre, M., Viitaniemi, K., D'Amico, G., Miao, Z., Unnithan, R.V.M., Vaccaro, A., van Hooren, L., et al. (2020). Platelet-Specific PDGFB Ablation Impairs Tumor Vessel Integrity and Promotes Metastasis. Cancer Res. *80*, 3345–3358. https://doi.org/10.1158/0008-5472.CAN-19-3533.
53. Wang, J.C., Li, G.Y., Wang, B., Han, S.X., Sun, X., Jiang, Y.N., Shen, Y.W., Zhou, C., Feng, J., Lu, S.Y., et al. (2019). Metformin inhibits metastatic breast cancer progression and improves chemosensitivity by inducing vessel normalization via PDGF-B downregulation. J. Exp. Clin. Cancer Res. *38*, 235. https://doi.org/10.1186/s13046-019-1211-2.
54. Qian, C., Yang, C., Tang, Y., Zheng, W., Zhou, Y., Zhang, S., Song, M., Cheng, P., Wei, Z., Zhong, C., et al. (2022). Pharmacological manipulation of Ezh2 with salvianolic acid B results in tumor vascular normalization and synergizes with cisplatin and T cell-mediated immunotherapy. Pharmacol. Res. *182*, 106333. https://doi.org/10.1016/j.phrs.2022.106333.
55. Baghaki, S., Yalcin, C.E., Baghaki, H.S., Aydin, S.Y., Daghan, B., and Yavuz, E. (2020). COX2 inhibition in the treatment of COVID-19: Review of literature to propose repositioning of celecoxib for randomized controlled studies. Int. J. Infect. Dis. *101*, 29–32. https://doi.org/10.1016/j.ijid.2020.09.1466.
56. Hayashi, T., Fujita, K., Nojima, S., Hayashi, Y., Nakano, K., Ishizuya, Y., Wang, C., Yamamoto, Y., Kinouchi, T., Matsuzaki, K., et al. (2018). High-Fat Diet-Induced Inflammation Accelerates Prostate Cancer Growth via IL6 Signaling. Clin. Cancer Res. *24*, 4309–4318. https://doi.org/10.1158/1078-0432.CCR-18-0106.
57. Tullemans, B.M.E., Heemskerk, J.W.M., and Kuijpers, M.J.E. (2018). Acquired platelet antagonism: off-target antiplatelet effects of malignancy treatment with tyrosine kinase inhibitors. J. Thromb. Haemostasis *16*, 1686–1699. https://doi.org/10.1111/jth.14225.
58. Elaskalani, O., Berndt, M.C., Falasca, M., and Metharom, P. (2017). Targeting Platelets for the Treatment of Cancer. Cancers *9*, 94. https://doi.org/10.3390/cancers9070094.

STAR★METHODS

KEY RESOURCES TABLE

REAGENT or RESOURCE	SOURCE	IDENTIFIER
Antibodies		
Anti-mouse COX2	Santa Cruz	Cat#sc-376861; RRID: AB_2722522
Anti-mouse CD36	Santa Cruz	Cat#sc-7309; RRID: AB_627044
Anti-mouse E-cadherin	Santa Cruz	Cat#sc-8426; RRID: AB_626780
Anti-rabbit COX2	Abcam	Cat#ab179800; RRID: AB_2894871
Gt Rb IgG H&L Alexa Fluor 594	Abcam	Cat#ab150080; RRID: AB_2650602
Anti-rabbit GAPDH	Proteintech	Cat#10494-1; RRID: AB_2263076
Anti-rabbit Ki67	Proteintech	Cat#27309-1; RRID: AB_2756525
Gt Ms IgG H&L Alexa Fluor 488	Proteintech	Cat#sa00013-1; RRID: AB_2810983
Anti-rabbit PTGS2	ABclonal	Cat#A3560; RRID: AB_2922972
FITC anti-human CD61	Biolegend	Cat#336403; RRID: AB_1227581
PE anti-human CD62P	Biolegend	Cat#304905; RRID: AB_314477
Anti-mouse N-cadherin	Cell Signaling Technology	Cat#14215; RRID: AB_2798427
Gt Rb IgG(H + L) HRP	Bioworld	Cat#BS13278; RRID: AB_2773728
Gt Ms IgG(H + L) HRP	Bioworld	Cat#BS12478; RRID: AB_2773727
Chemicals, peptides, and recombinant proteins		
Thrombin	Bio-sharp	Cat#BS903
Celecoxib	MCE	Cat#HY-14398
Imatinib	Selleck	Cat#STI571
Salvianolic acid B	Yuanye	Cat#S26732
DiI	Beyotime	Cat#C1036
Hoechst 33342	Beyotime	Cat#C1026
Fetal Bovine Serum	Gibco	Cat#10099
DMEM	Gibco	Cat#31600091
Penicillin-Streptomycin Solution	Corning	Cat#30-001-CI
Lipofectamine 2000 reagent	Thermo Fisher Scientific	Cat#11668500
crystal violet	LEAGENE	Cat#DZ0053
RIPA lysis buffer	KANGWAY	Cat#10243
Experimental models: Organisms/strains		
BALB/c mice	SiPeiFu	Cat#SCXK2019-0010
Critical commercial assays		
human peripheral blood platelet isolation kit	TBD	Cat#PLA2014
mouse peripheral blood platelet isolation kit	TBD	Cat#PLA2011M
BCA assay kit	Thermo Fisher Scientific	Cat#23225
enhanced chemiluminescent kit	Bio-sharp	Cat#BL520A
Total RNA extraction reagent	Vazyme	Cat#R104-01
Oligonucleotides		
shRNA against mouse COX-2	Corues	Cat#MC006
Software and algorithms		
FlowJo	BD	Version 10.4.1
Prism	GraphPad Software	Version 8.0.0

(*Continued on next page*)

Continued

REAGENT or RESOURCE	SOURCE	IDENTIFIER
ImageJ	NIH	RRID:SCR_003070
Other		
4T1-LUC cell line	ATCC	CRL-2539-LUC2; RRID: CVCL_J239
MDA-MB-231 cell line	ATCC	CRM-HTB-26; RRID: CVCL_0062
Leica SP8 STED 3X microscope	Leica	https://www.leica-microsystems.com.cn/cn/products/confocal-microscopes/p/leica-tcs-sp8-sted-one/
Zeiss Axio vert A1 microscope	Zeiss	https://www.zeiss.com.cn/microscopy/products/light-microscopes/axio-vert-a1-materials.html
HITACHI U8010 microscope	HITACHI	https://www.hitachi-hightech.com/cn/zhcn/products/microscopes/sem-tem-stem/fe-sem/regulus.html
FACS cytometer	Beckman	https://www.beckman.com/flow-cytometry/research-flow-cytometers/cytoflex/c09748

RESOURCE AVAILABILITY

Lead contact

Further information and requests for resources and reagents should be directed and will be fulfilled by the lead contact, Aiyun Wang (wangaiyun@njucm.edu.cn).

Materials availability

This study did not generate new unique reagents.

Data and code availability

- This study did not generate unique datasets or code.
- This study did not generate new unique reagents, cell lines, or mouse lines.
- Any additional information required to reanalyzed the data reported in this paper is available from the lead contact upon request.

EXPERIMENTAL MODEL AND STUDY PARTICIPANT DETAILS

Study approval

Whole blood samples were obtained from 15 healthy female volunteers (obtained after informed consent). All experiments were conducted with adherence to the Animal Committee of Nanjing University of Chinese Medicine (ethical review number: 202206A038). All tumor samples from 20 breast cancer patients (age: 46–68) were collected from Jurong People Hospital, as approved by the Jurong People Hospital Ethical Committee (permit and approval number: 2022-LS-003).

Animals

7-week-old female BALB/c mice were supplied by Beijing SiPeiFu Biotechnology Co., LTD (license number: SCXK2019-0010, Beijing, China). The approval of all animal studies was granted by the Animal Committee of Nanjing University of Chinese Medicine (ethical review number: 202206A038). The experiments were carried out as per the institutional guidelines of the Nanjing University of Chinese Medicine. The mice were kept in ventilated cages with solid bottoms at room temperature under a 12-h dark/light cycle.

The mouse breast cancer model was developed by injecting 2×10^5 4T1-luc cells intravenously in the absence and presence of 1×10^7 platelets in 100 μL PBS. After injection, the mice bearing 4T1-luc tumors were administered daily intraperitoneal injections of imatinib (20 mg/kg), Sal B (20 mg/kg), celecoxib (20 mg/kg), Sal B (20 mg/kg) + celecoxib (20 mg/kg) or an equal volume of saline (n = 5 in each group). After three weeks of treatment, the mice were euthanized to collect the lungs, which were further examined by H&E, immunofluorescence (IF), and immunohistochemistry (IHC) staining.

METHOD DETAILS

Cell culture

The authenticated 4T1 murine breast cancer cell line, luciferase-expressing 4T1-Luc cell line and MDA-MB-231 human breast adenocarcinoma cell line were obtained from American Type Culture Collection (Rockville, USA). All cell lines were cultured at 37°C with 5% CO_2 in DMEM supplemented with 10% Fetal Bovine Serum (FBS) (Gibco, USA), and 1% Penicillin-Streptomycin Solution (Corning, NY, USA).

Patient samples

All tumor samples from 20 breast cancer patients were collected from Jurong People Hospital, including 11 patients with metastasis and 9 patients without metastasis, as approved by the Jurong People Hospital Ethical Committee (permit and approval number: 2022-LS-003). The paraffin-embedded tissues from primary tumors were prepared at 4 μm sections for subsequent analysis. Hematoxylin and eosin (H&E) stained human breast cancer sections were independently and blindly scored by two pathologists.

Plasmid transfection

Small hairpin RNA (shRNA) for COX-2 was transfected into 4T1 cells using Lipofectamine 2000 reagent (Thermo Fisher Scientific, Waltham, USA). Cells were harvested 3 days after transfection for the further experiments. COX-2 knockdown plasmids were constructed by Corues Biotechnology Company (Nanjing, China).

Platelet isolation

Whole blood samples were acquired from 15 healthy female volunteers (obtained after informed consent). The enrolled subjects did not take aspirin or other nonsteroidal anti-inflammatory drugs for at least ten days before the blood draw. Whole blood was collected in citrate anti-coagulant tubes. Platelets from humans or mice were extracted by a human peripheral blood platelet isolation kit (PLA2014, TBD, China) or mouse peripheral blood platelet isolation kit (PLA2011M, TBD, China) as per the provided guidelines.

CCK8 assay

The breast cancer cells, pre-incubated with platelets or platelets CM or tested drugs, were plated in a 96-well plate at the density of 5,000 cells/well. Next, the cells were maintained with 10 μL of CCK-8 for 1.5 h at 37°C following the manufacturer's instructions (Beierbo, Nanjing, China). The optical density values were measured at 450 nm using a microplate reader (Biotek Synergy 2, Vermont, USA).

Enzyme-linked immunosorbent assay (ELISA)

After the treatment of tested drugs, the supernatants from activated platelets were collected. The secretion of PDGF-B in the cell supernatants was examined using a human PDGF-B ELISA kit (EK9137-96, MULTI SCIENCES, Zhejiang, China) according to the manufacturer's instructions. Similarly, the supernatants from the peripheral blood of mice were also collected. The concentrations of IL-6,IL-1β, and TNF-a in the supernatants were determined by using commercial ELISA kits (EK206 , EK201B , EK282 , MULTI SCIENCES, Zhejiang, China), according to the manufacturer's instructions. The absorbance was measured by using a microplate reader at 450 nm and 630 nm.

Wound healing and transwell migration assays

The treated 4T1 and MDA-MB-231 cells were seeded into a 6-well plate and incubated at 37°C overnight, after which the cells (85%–95% confluence) were carefully scraped out utilizing a 200 μL pipette tip. Each well was washed with PBS twice to smooth the edges of the scratches and remove the floating cells. Subsequently, the medium containing the tested drugs was added to the wells. The imaging of the plate was conducted at the same location using an inverted optical microscope (Zeiss Axio vert A1, Oberkochen, Germany). The gap was measured at 0 h (t1), and 24 h (t2), and the relative mobility (%) was derived based on the formula: (t1-t2)/t1×100%.

In terms of transwell migration assay, 6×10^4 MDA-MB-231 cells or 5×10^5 4T1 cells in 200 μL of serum-free or drug-containing medium were introduced into the upper chamber of a transwell insert, and 600 μL of the serum-containing medium was added into the lower chamber of transwell plates (3422, Corning, USA). After 24 h incubation, the cells were fixed with 600 μL methanol for 30 min. Subsequently, the cells were stained with 600 μL 0.1% crystal violet (LEAGENE, Beijing) for 30 min. The micrographs were imaged at 10× magnification under a microscope (Zeiss Axio vert A1, Oberkochen, Germany). The stained cells were quantified from three random fields.

Western blotting

The breast cancer cells were detached via a cell scraper and lysed with ice-cold RIPA lysis buffer (10243, KANGWAY, Shanghai, China) containing a protease inhibitor cocktail (89100146, DINGGUO, Beijing, China) at 4°C for 40 min. The supernatants were then collected after centrifugation at 12,000g for 15 min at 4°C. The total protein was quantified utilizing a BCA assay kit (Thermo Fisher Scientific, Waltham, USA). Equal amounts of proteins from each sample were separated into polyvinylidene difluoride (PVDF) membranes utilizing 10% SDS-polyacrylamide gels (Yeasen, Shanghai, China). The PVDF membranes were blocked in TBS (Tris-buffered saline) containing 3% milk powder and 0.2% Tween for 90 min. Subsequently, the membranes were subjected to incubation with the indicated primary antibodies at 4°C overnight. Afterward, the membranes were rinsed and exposed to the corresponding secondary antibodies for 2 h at room temperature. Finally, the protein bands were developed utilizing an enhanced chemiluminescent (ECL) kit (Bio-sharp, Wuhan, China). The intensities of Western blot bands were quantified using ImageJ software.

Co-culture system

The breast cancer cells were seeded into confocal mini-dishes in a mixture of medium and matrigel at a ratio of 2:1. After the solidification of tumor spheres, the drug-containing medium was added to the dishes. The dishes were imaged under an inverted optical microscope (Zeiss Axio vert A1, Oberkochen, Germany) at 0 h and 24 h.

Clot retraction assay

The platelet suspension was treated with various concentrations of Sal B and adjusted to 1 mL (platelets: 5×10^7/mL) with Tyrode's buffer containing 10 mM GSH (L-Glutathione reduced). The washed red blood cells and the CM from MDA-MB-231 cells were then added to initiate the formation of fibrin clots. Clot formation and retraction were examined within 45 min at 37°C with the addition of a glass capillary. The weights of the blood clot and the squeezed serum were measured as signs of blood clot retraction.

Platelet adhesion and aggregation assays

Collagen I solution (100 μg/mL, 150 μL) was applied to 24-well plates in advance for coating. The collagen I supernatants were discarded 12 h later and the 24-well plates were airdried. 5×10^7/mL Dil-labeled platelets resuspended in the buffer were incubated with Sal B for 40 min. Next, 100 μL platelet solution was incubated in the collagen-coated 24-well plate for 30 min at 37°C and then washed with buffer. Three fields were randomly selected and imaged under a fluorescence microscope (Zeiss Axio vert A1, Oberkochen, Germany) to analyze the number and the aggregation of platelets.

Hemocyte sedimentation and coagulation index examination

Whole blood or platelet-rich plasma samples were collected from healthy volunteers, and then the samples were incubated with different concentrations of Sal B for 30 min, followed by the incubation with CM from MDA-MB-231 cells for 15 min. Hemocyte sedimentation rate was measured in a whole blood automatic analyzer and four types of coagulation indexes (APTT, PT, TT and FIB) were measured by an automatic hemagglutination apparatus.

Quantitative RT-PCR

Total RNA was isolated from the platelets using total RNA extraction reagent Reagent (Vazyme, Nanjing, China). An aliquot of 5 μg RNA was reverse-transcribed into cDNA utilizing a HiScript II QRT SuperMix for qPCR (Vazyme, Nanjing, China). SYBR Green real-time PCR amplification and detection were carried out with the aid of an ABI 7500 system (Applied Biosystems, Waltham, USA). mRNA expression levels were evaluated utilizing the $^{2-\Delta\Delta}$Ct method. GAPDH was utilized as a control. Primers used in this research are listed in Table S1.

Flow cytometry

Flow cytometry was utilized to examine the activation of platelets by analyzing the expression levels of CD61 and CD62P. The treated platelets were stained with antibodies against CD61 and CD62P for 30 min at 4°C in the dark. Subsequently, the stained platelets were centrifuged and washed. The cells were sorted on a FACS cytometer (Beckman cytoflex, Brea, USA) and assessed utilizing the FlowJo software (Franklin Lake, USA).

Scanning electron microscopy (SEM)

Platelets and breast cancer cells were fixed with a mixed solution containing 2% paraformaldehyde (PFA) and 4% glutaraldehyde. Samples were rinsed with 0.1 mol/L PBS and soaked in 1% osmic acid-0.1 mol/L PBS for 30 min, followed by rinse with 0.1 mol/L PBS and then dehydration by gradient ethanol. The cells were immersed in isoamyl acetate for 20 min and then transferred to a desiccator. Finally, a SEM (HITACHI U8010, Tokyo, Japan) was used to observe samples and images were taken for analysis.

IHC staining

The lung or tumor tissue sections harvested from mice or breast cancer patients were initially deparaffinized with xylene and rehydrated, after which antigen retrieval was performed in the 10 mM sodium citrate and 0.05% Tween for 3 min at 95°C. The sections were then blocked with 5% bovine serum albumin (BSA) solution for 30 min and incubated with indicated primary antibodies at 4°C overnight, followed by incubation with the corresponding secondary antibodies for 2 h at room temperature. Finally, the sections were stained with 3, 3′-dia-minobenzidine (DAB), sealed with a neutral gum, and observed under a microscope (Olympus, Japan) at 40× magnification. The IHC signals were photographed and the images were analyzed using ImageJ software (National Institutes of Health, USA).

IF staining

The lung or tumor tissue sections were dissociated in xylene, dehydrated in an ethyl alcohol gradient, and subjected to antigen retrieval in a sodium citrate solution (Servicebio, Wuhan, China) in a microwave. The sections with indicated primary antibodies were cultured overnight at 4°C and then incubated with corresponding secondary antibodies for 2 h at room temperature. The sections were then stained with Hoechst33342 to label nuclei. Three to five random fields per sample were selected and imaged under a Zeiss microscopy (Zeiss Axio vert A1, Oberkochen, Germany). The images were analyzed by ImageJ software (National Institutes of Health, USA).

In terms of cell IF staining for cells, cells were fixed and incubated with the indicated primary antibodies, followed by incubation with the corresponding fluorescent secondary antibodies. The nuclei were counterstained with Hoechst 33342, and the images were taken by a Leica SP8 confocal microscopy (Leica SP8 STED 3X, Heidelberg, Germany).

H&E staining

The harvested lung and liver tissues were washed with PBS and then fixed with 4% PFA overnight. These tissues were washed in gradient ethanol and xylene, followed by embedded in paraffin. The samples were sectioned at 4 μm thickness and stained with H&E based on standard protocols. The sections were then imaged using Mantra Pathology Workstation (PerkinElmer, Waltham, USA).

Bioluminescence imaging for tumor monitoring

For *in vivo* imaging, the mice were anesthetized with isoflurane, followed by the intraperitoneal injection of 0.1 mL D-luciferin (10 mg/mL, 115144-35-9, CSNpharm, Chicago, USA) 5min before live imaging. The images were acquired using the IVIS Spectrum imaging system (PerkinElmer, USA). In light of *ex vivo* tissue imaging, the tumor-bearing mice were perfused with PBS. The tissues were then harvested, followed by the incubation with 5 mg/mL D-luciferin in PBS. The analysis was performed using the Living Image 4.5 software (Version4.5, Waltham, USA).

Detection of circulating tumor cells (CTCs)

To detect CTCs, the tumor-bearing mice were anesthetized with isoflurane, and the whole blood of mice was collected through cardiac puncture with needles of 1 mL syringes containing 50 μL EDTA (0.5 M). The total blood cells were separated from plasma by the centrifugation at 1,500g for 5 min at 4°C. After discarding the supernatants, the cell pellets were resuspended in 1 mL erythrocyte lysis buffer and incubated for 20 min at room temperature. After another centrifugation step at 500 g for 10 min at room temperature, the supernatants were discarded. Subsequently, and cells were resuspended again in 1 mL of erythrocyte lysis buffer and incubated for 15 min before spinning down one more time for 10 min at 400 g. The cell pellets were then washed once in 1 mL D10F, spun down for 10 min at 400 g, resuspended in D10F and plated on a culture dish. The bioluminescence of individual tissue culture plate was measured using the IVIS Spectrum Imaging System (PerkinElmer, Waltham, USA) 10 days following blood collection.

Bioinformatics analysis

In terms of bioinformatics analysis, we found GSE2603 gene chips from the GEO database (https://www.ncbi.nlm.nih.gov). Differentially expressed gene volcano plot and heatmap were made by Hiplot (https://hiplot.com.cn/).

QUANTIFICATION AND STATISTICAL ANALYSIS

Statistical analysis

Unless otherwise indicated, all data were presented as mean ± standard deviation (SD). Statistical analysis was performed using GraphPad Prism software (Version8.0, San Diego, USA), on the basis of unpaired Student's test for comparisons between two groups and one-way ANOVA analysis for more than two groups. p values were denoted in figures as: not significant [ns], $p > 0.05$, *$p < 0.05$, **$p < 0.01$, ***$p < 0.001$. The quantification of staining images and blot images were analyzed using ImageJ software (National Institutes of Health, USA). Flow cytometry analysis were analyzed using FlowJo software (Version10.4.1, Franklin Lake, USA).